J. Fluid Mech. (1998), *vol.* 368, *pp.* 229–262. Printed in the United Kingdom

Cellular detonation stability. Part 1. A normal-mode linear analysis

By MARK SHORT AND D. SCOTT STEWART

Theoretical and Applied Mechanics, University of Illinois, Urbana, IL 61801, USA

(Received 24 September 1997 and in revised form 23 March 1998)

A detailed investigation of the hydrodynamic stability to transverse linear disturbances of a steady, one-dimensional detonation in an ideal gas undergoing an irreversible, unimolecular reaction with an Arrhenius rate constant is conducted via a normal-mode analysis. The method of solution is an iterative shooting technique which integrates between the detonation shock and the reaction equilibrium point. Variations in the disturbance growth rates and frequencies with transverse wavenumber, together with two-dimensional neutral stability curves and boundaries for all unstable low- and higher frequency modes, are obtained for varying detonation bifurcation parameters. These include the detonation overdrive, chemical heat release and reaction activation energy. Spatial perturbation eigenfunction behaviour and phase and group velocities are also obtained for selected sets of unstable modes. Results are presented for both Chapman–Jouguet and overdriven detonation velocities. Comparisons between the earlier pointwise determination of stability and interpolated neutral stability boundaries obtained by Erpenbeck are made. Possible physical mechanisms which govern the wavenumber selection underlying the initial onset of either regular or irregular cell patterns are also discussed.

1. Introduction

Detonation waves propagating in a rectangular channel reveal a well-known pattern of cellular instability (Fickett & Davis 1979). These cell, or diamond, patterns arise from intense regions of vorticity known as triple points associated with the intersection of incident and Mach stem shocks, which comprise the detonation front, with a reflected shock, which propagates transverse to the detonation front. The triple points etch their locus onto soot-covered foil attached to the channel walls, enabling the determination of detonation cell sizes for various channel widths, initial conditions and reaction mixtures (see e.g. Strehlow 1969, 1970; Lee 1984). A database of these extensive experimental records has recently been established by Kaneshige, Shepherd & Teodorczyk (1997). Of central importance in developing a mathematical model describing the evolution dynamics of the cellular detonation formation process is a comprehensive understanding of the multi-dimensional linear stability behaviour of a steady planar detonation wave for varying bifurcation parameters. These include the activation energy or energies of the chemical reaction, the chemical heat release parameters and the detonation velocity.

Most of the current results on the hydrodynamic response to linear transverse disturbances of a steady, planar detonation in an ideal gas undergoing an irreversible unimolecular reaction with an Arrhenius rate factor, the now standard idealized

detonation model, were obtained by Erpenbeck (1962*a*, 1964, 1965, 1966, 1970). In his Laplace transform formulation, stability or instability was determined pointwise and interpolation was used to estimate neutral stability boundaries. Almost no information regarding the number of unstable perturbation modes, their growth rates, frequencies and eigenfunction structures for a given parameter set was obtained. These features must be calculated if an understanding of the dynamics of cell formation is to be obtained. Nevertheless, a major contribution of Erpenbeck was to identify an approximate range of transverse wavenumbers, for various system parameters, over which the model system was linearly unstable.

In contrast to Erpenbeck's formulation, Lee & Stewart (1990*a*) used a normal-mode approach for the one-dimensional linear detonation stability problem, employing a two-point numerical boundary-value shooting algorithm to determine unstable mode growth rates, frequencies, and perturbation eigenfunction structures. Lee & Stewart (1990*b*), Bourlioux & Majda (1992) and Short (1997*a*) have presented growth-rate versus wavenumber behaviour using the normal-mode approach for some limited ranges of two-dimensional disturbances, but no extensive systematic study to understand multi-dimensional linear stability in the context of a regular bifurcation problem has yet been conducted. In addition to these numerical studies, an asymptotic analysis of linear stability to periodic disturbances in the limit of small wavelength was undertaken by Erpenbeck (1966). Buckmaster (1989), Short (1996, 1997*b*) and Short & Stewart (1997) have derived analytical approximations to the stability behaviour when a finite wavenumber band of low-frequency instability is present through an asymptotic analysis based on a large activation energy and, in the case of Short (1996, 1997*b*) and Short & Stewart (1997), a ratio of specific heats close to unity. Analytical estimates of the initial detonation cell spacing were also given by these authors based on the wavelength corresponding to the maximum growth rate of the low-frequency, fundamental, mode.

Mathematical analyses which predict a nonlinear detonation cell spacing have also been conducted. Strehlow & Fernandes (1966), Barthel & Strehlow (1966) and Barthel (1974), with a formal asymptotic analysis by Majda (1987), established estimates based on propagation dynamics of high-frequency disturbances using acoustic ray tracing. However, both the experimental (Strehlow, Maurer & Rajan 1969; Barthel 1974) and numerical evidence (Bourlioux & Majda 1992) is that the actual cell sizes differ by several orders of magnitude from those predicted by the high-frequency theory, indicating that high-frequency disturbances probably play only a minor role in the dynamics of cellular detonation formation. In contrast, weakly nonlinear, long-wavelength evolution equations aimed at modelling cellular patterns near a neutral stability boundary have been developed by Erpenbeck (1970) and by Majda & Roytburd (1992), but no complete comparison of the results obtained from these equations with numerical experiments has yet been made. A recent large-activation-energy, low-frequency, long-wavelength analysis by Yao & Stewart (1996) has led to the derivation of a third-order evolution equation which does predict cellular detonation solutions (Stewart, Aslam & Yao 1996). The long-time weakly nonlinear cells are found to have a wavelength corresponding to the low-wavenumber linear neutral stability boundary, where both the phase and group velocities are also a maximum. However, as will be shown below, typical linear detonation stability spectra have several features that are not present in the linear dispersion relation corresponding to the Stewart–Yao equation, and thus a physical mechanism that defines an initial cell spacing is difficult to interpret.

In order to further our understanding of the cellular detonation instability problem, highly resolved numerical simulations of the initial stages of cellular detonation

formation are now required to be conducted in conjunction with a comprehensive knowledge of the corresponding linear stability behaviour. Such investigations have been very successful in understanding the dynamics of one-dimensional pulsating detonation instabilities (Fickett & Wood 1966; Bourlioux, Majda & Roytburd 1991; Short & Quirk 1997). Bourlioux & Majda (1992) and Quirk (1994) have conducted some limited experiments of this type for detonations propagating in a two-dimensional channel, but the restricted size of the channel poses some difficulties when comparing the results with the linear stability behaviour, which assumes an infinite transverse domain.

The present analysis is the first in a set of two studies with the aim of understanding the dynamics of the initial cellular detonation formation process. We emphasize that our concern is not with the complex dynamics of the fully nonlinear cellular problem, but with the potentially solvable problem of understanding how weak detonation cells develop from a small initial disturbance. We restrict our attention to a one-step Arrhenius reaction model, in contrast to the model three-step chain-branching kinetics studied by Short & Quirk (1997), since it is the simplest realistic reaction model that minimizes the number of bifurcation parameters. Nevertheless, this model allows us to understand the general effects on the detonation stability behaviour brought about by changes in the detonation overdrive, the heat release and the activation energy of the reaction. In the following, a detailed investigation of the hydrodynamic linear stability to periodic transverse disturbances for a steady, planar detonation is made. Particular attention is paid to interpreting the stability behaviour for varying bifurcation parameters relative to associated changes in the structure of the underlying planar, steady detonation wave. The linear stability equations are solved numerically by the implementation of the normal-mode, two-point boundary shooting algorithm described in Short (1997*a*), which was first formulated in Lee & Stewart (1990*a*). Complete growth-rate and frequency behaviour with transverse wavenumber, two-dimensional neutral stability curves and boundaries, spatial perturbation eigenfunction behaviour, and phase and group velocities for various sets of unstable low-frequency and higher frequency modes are calculated. A particular emphasis of the present study is identifying and interpreting those features, such as the appearance of additional higher frequency unstable modes as regions of greater instability are encountered, which will influence the physics of the initial cell formation process. The second study (Quirk & Short 1998) is a numerical investigation of the nonlinear mechanisms behind the initial stages of cellular detonation formation in very wide channels, conducted in specific relation to the linear stability results obtained here.

2. Model

An ideal gas $\mathscr{F}$ is assumed to undergo the unimolecular, first-order, irreversible reaction

$$\mathscr{F} \rightarrow \mathscr{P}$$

to product $\mathscr{P}$ with constant mole fraction and ratio of specific heats γ. The reaction rate is modelled by one-step Arrhenius kinetics where the rate equation for the reaction progress variable, λ, is

$$\frac{\mathrm{D}\lambda}{\mathrm{D}t} = r = K(1-\lambda)\exp\left[-\theta/\left(p/\rho\right)\right]. \tag{2.1}$$

Here θ is the non-dimensional activation energy for the reaction, K the non-dimensional pre-exponential factor, and p, ρ the non-dimensional pressure and density,

respectively. The model assumes that K is a constant. Unburnt fuel corresponds to $\lambda = 0$, fully depleted fuel to $\lambda = 1$. The convective derivative is

$$\frac{\mathrm{D}}{\mathrm{D}t} = \frac{\partial}{\partial t^l} + u_1^l \frac{\partial}{\partial x^l} + u_2^l \frac{\partial}{\partial y^l},$$

where the superscript l on Cartesian space coordinates (x, y), on velocity components (u_1, u_2) and on the time coordinate t denotes the laboratory frame. The caloric and ideal thermal equations of state are respectively

$$e = \frac{p}{(\gamma - 1)\rho} - q, \quad T = p/\rho, \tag{2.2}$$

for specific internal energy e, temperature T and local chemical energy q, where

$$q = \beta\lambda. \tag{2.3}$$

Here β represents the total chemical energy available in the unreacted mixture. Finally, the model is completed by assuming the hydrodynamic behaviour of the fluid to obey the compressible reactive Euler equations in which heat-conduction, viscosity and radiation effects are negligible. In non-dimensional form these are

$$\frac{\mathrm{D}\rho}{\mathrm{D}t} + \rho\nabla\cdot\boldsymbol{u}^l = 0, \quad \frac{\mathrm{D}\boldsymbol{u}^l}{\mathrm{D}t} + v\nabla p = 0, \quad \frac{\mathrm{D}e}{\mathrm{D}t} + p\frac{\mathrm{D}v}{\mathrm{D}t} = 0, \tag{2.4}$$

with the velocity vector $\boldsymbol{u}^l = (u_1^l, u_2^l)$ and the specific volume $v = \rho^{-1}$.

The scales for density, pressure, temperature and velocity are the dimensional post-shock density, pressure, temperature and sound speed ($\tilde{c}_s^*$) respectively in an appropriately defined steady detonation wave. The scaling for length is the steady half-reaction length ($\tilde{l}_{1/2}$), the distance from the shock to the point where half of the reactant is consumed, and for time, $\tilde{c}_s^*\tilde{l}_{1/2}$. The scaled activation energy and heat release quantities θ and β are defined as

$$\theta = \frac{\gamma\widetilde{E}}{\tilde{c}_s^{*\,2}}, \quad \beta = \frac{\gamma\widetilde{Q}}{\tilde{c}_s^{*\,2}}, \tag{2.5}$$

for dimensional activation energy $\widetilde{E}$ and heat release $\widetilde{Q}$. An alternative is the scaled activation energy E and heat release Q due to Erpenbeck (1964) defined as

$$E = \frac{\gamma\widetilde{E}}{\tilde{c}_0^{*\,2}}, \quad Q = \frac{\gamma\widetilde{Q}}{\tilde{c}_0^{*\,2}}, \tag{2.6}$$

where $\tilde{c}_0^*$ is the adiabatic pre-shock sound speed. Defined in this way, E and Q are independent of the detonation speed but as will be demonstrated below, θ and β are better suited to describing the steady detonation structure and thus its stability behaviour.

3. Steady detonation structure

The standard reactive flow model described in §2 admits a steady, one-dimensional steady-wave solution, denoted in the following by the superscript $*$, whose spatial structure can be determined through a Rankine–Hugoniot analysis together with the rate law (2.1). Assuming the steady detonation to propagate to the left along the path $x^l = -D_s^* t^l$, where D_s^* is the steady detonation Mach number relative to the

post-shock sound speed, the pressure, velocity and density can be shown to satisfy

$$p^* = a + (1-a)\left(1 - bq^*\right)^{1/2}, \quad u_1^* = \frac{(1-p^*)}{\gamma M_s^*} + M_s^*, \quad u_2^* = 0, \quad \rho^* = \frac{M_s^*}{u_1^*}, \tag{3.1}$$

in the steady shock-attached coordinate system

$$X = x^l + D_s^* t^l, \tag{3.2}$$

where

$$M_s^{*2} = \frac{(\gamma-1)D^{*2}+2}{2\gamma D^{*2}-(\gamma-1)}, \quad a = \frac{\gamma M_s^{*2}+1}{(\gamma+1)}, \quad b = \frac{M_s^{*2}2\gamma(\gamma-1)}{(1-a)^2(\gamma+1)}. \tag{3.3}$$

The quantity D^* denotes the detonation Mach number relative to the upstream unreacted material, while M_s^* is the flow Mach number immediately behind the shock. The chemical energy release q^* in the steady wave satisfies

$$q^* = \beta\lambda^*. \tag{3.4}$$

The variation in the reaction progress variable is determined by numerical quadrature of the first-order equation

$$\lambda_X^* = r^*/u_1^*, \tag{3.5}$$

which defines the pre-exponential factor K as

$$K = \int_0^{1/2} u_1^*(1-\lambda^*)^{-1} \exp\left[\theta/\left(p^*/\rho^*\right)\right] \mathrm{d}\lambda^*. \tag{3.6}$$

Given that the steady variables satisfy the shock conditions,

$$\rho^* = p^* = T^* = 1, \quad u_1^* = M_s^*, \quad u_2^* = 0, \quad \lambda^* = 0, \tag{3.7}$$

(3.5) may be integrated away from the shock at $X = 0$ to determine the complete structure of the steady detonation wave for $X > 0$. The detonation velocity D^* is determined by specification of the detonation overdrive,

$$f = \left(\frac{D^*}{D_{CJ}^*}\right)^2, \tag{3.8}$$

where D_{CJ}^* is the Chapman–Jouguet (CJ) detonation velocity, i.e. the minimum sustainable steady velocity determined by the flow velocity being exactly sonic, $M^* = 1$, at the end of the wave where $q^* = \beta$; here the local flow Mach number

$$M^* = \frac{u_1^*}{\left(p^*/\rho^*\right)^{1/2}}. \tag{3.9}$$

In terms of Q and γ,

$$D_{CJ}^* = \left[\left(1 + \frac{(\gamma^2-1)Q}{\gamma}\right) + \left(\left(1 + \frac{(\gamma^2-1)Q}{\gamma}\right) - 1\right)^{1/2}\right]^{1/2}. \tag{3.10}$$

These results define the steady Zeldovich–von Neumann–Döring (ZND) structure. We are now interested in understanding the changes in the steady wave structure as the bifurcation parameters, the detonation overdrive f, the activation energy E, the heat release Q, and their corresponding post-shock thermal energy scaled values θ and β, are varied. It will also be demonstrated that the reason θ and β better reflect the steady structure, and thus the corresponding stability behaviour, is due to the dependence

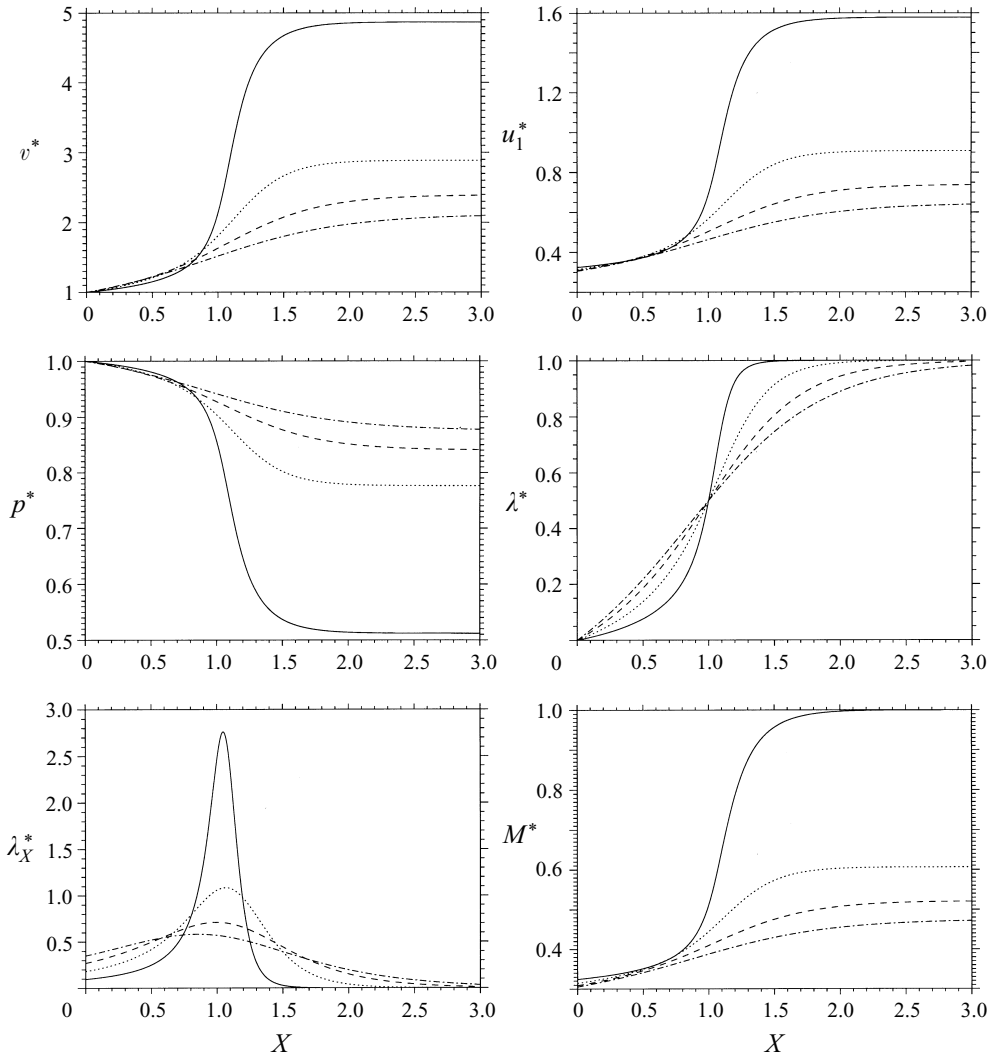

FIGURE 1. ZND profiles for $Q = 50$, $E = 50$, $\gamma = 1.2$, and $f = 1$ (solid), $f = 1.4$ (dotted), $f = 1.8$ (dashed) and $f = 2.2$ (dot-dash).

of both the reaction rate and the amplitude of thermodynamic variation between the detonation shock and equilibrium point on the velocity-dependent, post-shock steady state. For example, it is easily verified that a large E might not correspond to the classical square-wave type of profile that one normally associates with large activation energies, if the detonation velocity is also appropriately large.

3.1. *ZND profiles for varying overdrive f*

Figure 1 shows the change in the steady wave structure for $Q = 50$, $E = 50$, $\gamma = 1.2$ and for the increasing detonation overdrives $f = 1$, $f = 1.4$, $f = 1.8$ and $f = 2.2$. Table 1 shows the corresponding variation of β and θ as f is varied. For a fixed, pre-shock thermal-energy-scaled heat release Q, an increase in the detonation overdrive will result in a larger detonation velocity ($D^* = f^{1/2} D^*_{CJ}(Q,\gamma)$) and a thus relative increase in the post-shock thermal energy. Since β and θ are scaled with

f	β	θ
1.0	10.39	10.39
1.4	7.88	7.88
1.8	6.35	6.35
2.2	5.31	5.31

TABLE 1. Variation of β and θ with f for $Q = 50$, $E = 50$ and $\gamma = 1.2$

E	β	θ
50.0	10.39	10.39
37.5	10.39	7.79
25.0	10.39	5.19
12.5	10.39	2.60
0	10.39	0

TABLE 2. Variation of β and θ with E for $Q = 50$, $f = 1$ and $\gamma = 1.2$

respect to the post-shock value, there is a corresponding decrease in these values as f increases. The size of θ governs the sensitivity of the reaction rate to changes in the local thermodynamic state, while β governs the size of the thermodynamic variations which occur due to exothermicity of the reaction. An increase in θ implies a more state-sensitive reaction, while an increase in β implies larger thermodynamic variations due to chemical reaction.

As predicted, table 1 shows that the largest values of β and θ are obtained for the lowest overdrive $f = 1$. Figure 1 shows that the ZND profiles then approach those of a classical square-wave detonation structure, showing a clearly defined induction zone and main heat release layer (see λ_X^*). At this point, θ has the moderately large value $\theta = 10.39$. Descriptions of the steady variation in the induction and main heat release zones can be easily obtained by an asymptotic analysis assuming $\theta \gg 1$. As f increases, β and θ decrease, the peak reaction rate drops and the length of the steady wave, denoted by the region from the shock to the point where significant variations in λ^* cease to occur, increases. The ZND profiles also show the disappearance of the square-wave structure. For $f = 2.2$, $\theta = 5.31$, and the ZND profiles indicate an almost linear consumption of fuel behind the shock and a long relaxation tail before the burnt equilibrium zone is reached. Corresponding to the decrease in β, the thermodynamic variation through the wave is also weakened, with the pressure drop through the wave for $f = 2.2$ equal to 0.12, but equal to 0.49 for $f = 1$. In the limit of infinite overdrives, the detonation profiles approach the inert-Euler step-shock structure (Erpenbeck 1964).

3.2. *ZND profiles for varying activation energy E*

Figure 2 shows the change in the steady-wave structure for $Q = 50$, CJ detonation velocity $f = 1$, $\gamma = 1.2$ and for the decreasing activation energies $E = 50$, $E = 37.5$, $E = 25$, $E = 12.5$ and $E = 0$. Table 2 shows the corresponding variation of β and θ as E is varied. Since both the detonation velocity and equilibrium states are independent of E, the post-shock thermal energy remains constant and the variation in the profiles is due to the exponential dependence of the reaction rate on θ. As expected the square-wave profile is approached for larger E. As E, and hence θ decreases, the sensitivity of the reaction rate to changes in the local thermodynamic state is weakened. The peak in the maximum reaction rate drops significantly, and the

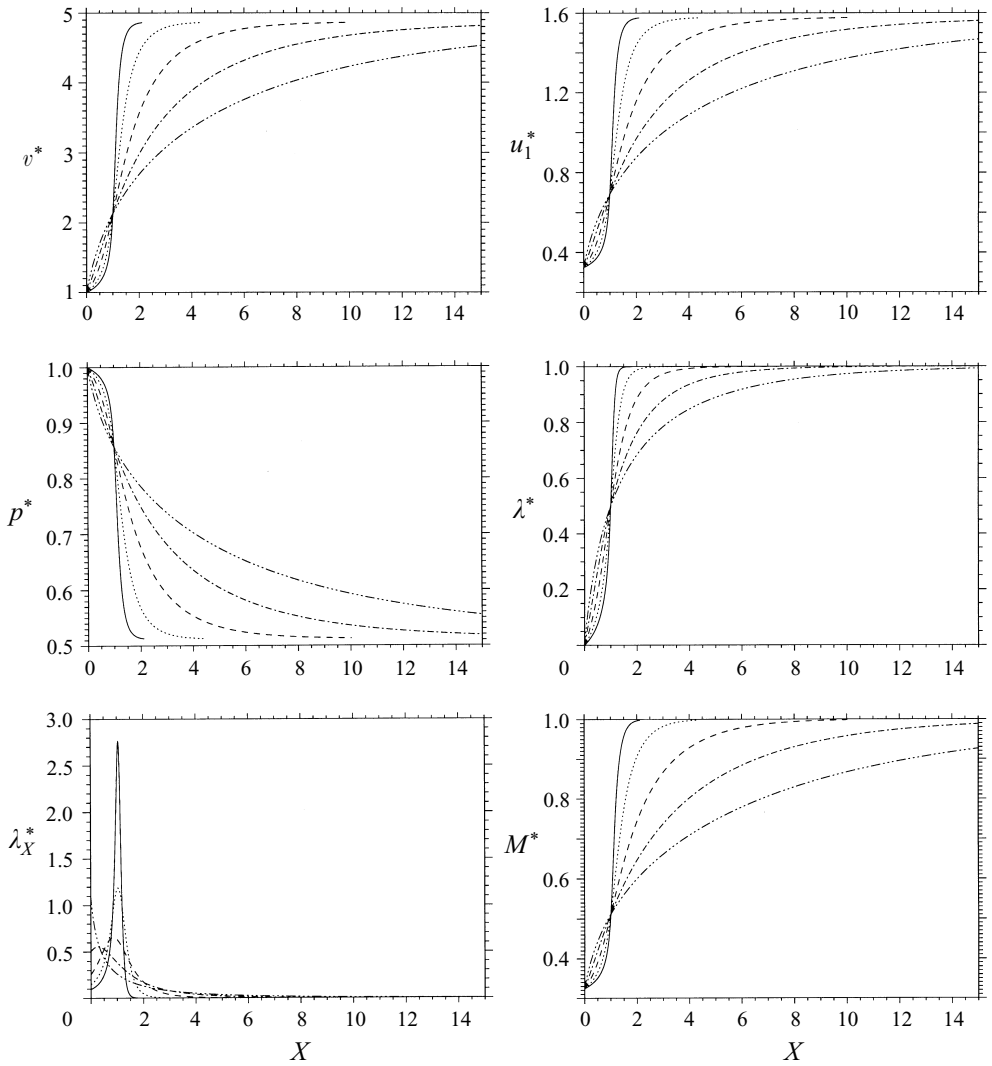

FIGURE 2. ZND profiles for $Q = 50$, $\gamma = 1.2$, $f = 1$, and $E = 50$ (solid), $E = 37.5$ (dotted), $E = 25.0$ (dashed), $E = 12.5$ (dash-dot) and $E = 0$ (dot-dot-dot-dash).

detonation structure is markedly lengthened. Again, the ZND profiles possess an ever lengthening relaxation tail, where for $E = 12.5$, $\theta = 2.60$, and the steady detonation is over seven times wider than that for $E = 50$. For $E = 0$, the exponential sensitivity of the reaction rate to thermodynamic state variations is absent.

3.3. *ZND profiles for varying heat release Q*

The final set of ZND profiles shown in figure 3 displays the changes which occur for $E = 50$, $\gamma = 1.2$, $f = 1.2$ and for the decreasing heat release values $Q = 50$, $Q = 37.5$, $Q = 25$, $Q = 12.5$ and $Q = 0$. Of particular note is the succinct manner in which the square-wave structure is adopted for decreasing Q. For $Q = 12.5$ there is a spatially thin main heat release layer attached to a weakly varying induction zone layer. Correspondingly, the reaction rate has a maximum value $\partial\lambda/\partial X = 43.35$ for

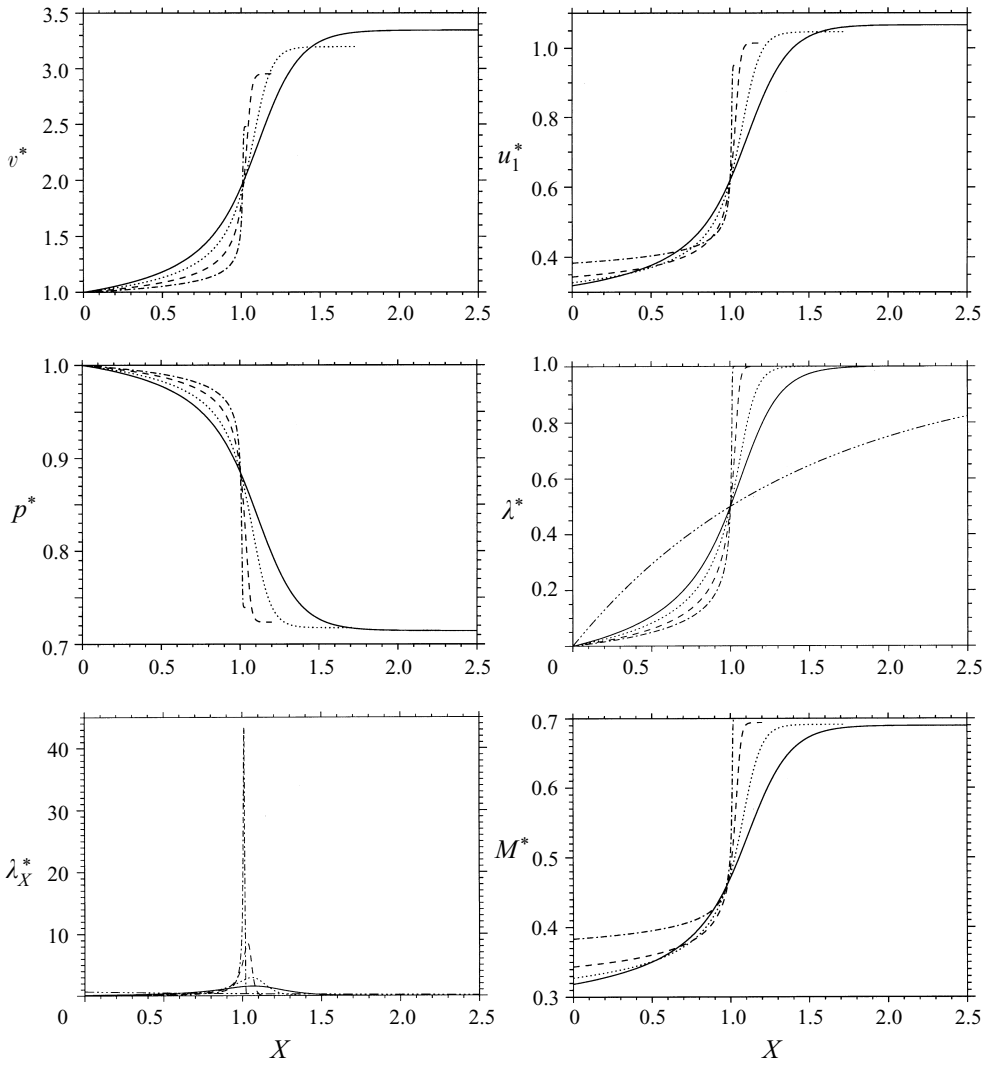

FIGURE 3. ZND profiles for $E = 50$, $\gamma = 1.2$, $f = 1.2$, and $Q = 50$ (solid), $Q = 37.5$ (dotted), $Q = 25.0$ (dashed), $Q = 12.5$ (dash-dot) and $Q = 0$ (dot-dot-dot-dash).

$Q = 12.5$ compared to a maximum value $\partial\lambda/\partial X = 1.57$ for $Q = 50$. The approach to the square-wave structure can be explained as follows: for decreasing Q at fixed overdrive, the relative detonation velocity must decrease. Consequently the thermal energy behind the shock is lowered and θ increases, increasing the sensitivity of the reaction, and resulting in the square-wave structure. The increase in θ for decreasing Q can be observed in table 3. For low Q, there is only a weak coupling between the exothermicity of chemical reaction and variations in the thermodynamic state. At $Q = 0$, the detonation structure simply comprises a standard inert-Euler step-shock profile. Although $\beta = Q = 0$ is a singular limit in this context, an analytical description of the steady wave structure can be easily obtained in terms of exponential integral functions by assuming an ordered limit between θ and β such that $\beta\theta = O(1)$ for $\beta \to 0$, $\theta \to \infty$. As $\beta\theta \to \infty$, the structure adopts the square-wave profile observed

Q	β	θ
50.0	8.96	8.96
37.5	8.36	11.14
25.0	7.37	14.73
12.5	5.44	21.78
0	0	48.37

TABLE 3. Variation of β and θ with Q for $E = 50$, $f = 1.2$ and $\gamma = 1.2$

for $Q = 12.5$. For $\beta\theta \to 0$, the structure adopts the limiting form for $Q = 0$ observed in figure 3.

4. Two-dimensional linear stability analysis

A normal-mode linear stability analysis of the steady detonation wave structure (3.1)–(3.7) for two-dimensional disturbances has been conducted. This proceeds by defining a shock-attached coordinate system

$$x = x^l + D_s^* t^l - \psi(y,t), \quad t = t^l, \tag{4.1}$$

where $\psi(y,t)$ represents the perturbation to the shock. Perturbations to the steady detonation wave structure are sought in the normal-mode form

$$\boldsymbol{z} = \boldsymbol{z}^*(x) + \boldsymbol{z}'(x)\mathrm{e}^{\alpha t + \mathrm{i}ky}, \quad \psi = \psi'\mathrm{e}^{\alpha t + \mathrm{i}ky}, \tag{4.2}$$

where

$$\boldsymbol{z} = [v,\ u_1,\ u_2,\ p,\ \lambda]^{\mathrm{T}}, \tag{4.3}$$

$\mathrm{Re}(\alpha)$ is the disturbance growth rate, $\mathrm{Im}(\alpha)$ is the disturbance frequency and k is the disturbance wavenumber. Substituting (4.1) and (4.2) into (3.1)–(3.7) results in a system of five first-order linear differential equations for the vector of complex perturbation eigenfunctions $\boldsymbol{z}'(x)$ which can be written in the form

$$\boldsymbol{A}^* \cdot \boldsymbol{\zeta}_{,x} + \left(\alpha + \mathrm{i}k\boldsymbol{B}^* \cdot + \boldsymbol{C}^* \cdot\right) \boldsymbol{\zeta} - \left(\alpha + \mathrm{i}k\boldsymbol{B}^* \cdot\right) \boldsymbol{z}_x^* = 0, \tag{4.4}$$

where

$$\boldsymbol{\zeta} = \boldsymbol{z}'/\psi'. \tag{4.5}$$

The matrices $\boldsymbol{A}^*$, $\boldsymbol{B}^*$ and $\boldsymbol{C}^*$ are

$$\boldsymbol{A}^* = \begin{bmatrix} u_1 & -v & 0 & 0 & 0 \\ 0 & u_1 & 0 & v/\gamma & 0 \\ 0 & 0 & u_1 & 0 & 0 \\ 0 & \gamma p & 0 & u_1 & 0 \\ 0 & 0 & 0 & 0 & u_1 \end{bmatrix}^*, \quad \boldsymbol{B}^* = \begin{bmatrix} u_2 & 0 & -v & 0 & 0 \\ 0 & u_2 & 0 & 0 & 0 \\ 0 & 0 & u_2 & v/\gamma & 0 \\ 0 & 0 & \gamma p & u_2 & 0 \\ 0 & 0 & 0 & 0 & u_2 \end{bmatrix}^*, \tag{4.6}$$

and

$$\boldsymbol{C}^* = \begin{bmatrix} -u_{1,x} & v_{,x} & 0 & 0 & 0 \\ p_{,x}/\gamma & u_{1,x} & 0 & 0 & 0 \\ 0 & u_{2,x} & 0 & 0 & 0 \\ -(\gamma-1)\beta[r_v - r/v]/v & p_{,x} & 0 & \gamma u_{1,x} - (\gamma-1)\beta r_p/v & -(\gamma-1)\beta r_\lambda/v \\ -r_v & \lambda_{,x} & 0 & -r_p & -r_\lambda \end{bmatrix}^*. \tag{4.7}$$

The undefined quantities in $\boldsymbol{C}^*$ are

$$r_v = \frac{r\theta}{vT}, \quad r_p = \frac{r\theta}{pT}, \quad r_\lambda = -K\exp\left(-\frac{\theta}{T}\right). \tag{4.8}$$

The perturbation shock conditions are determined from the linearized Rankine–Hugoniot shock relations as

$$\left.\begin{aligned} v' = \frac{4\alpha}{(\gamma+1)D^{*2}M_s^*}\psi', \quad u_1' = \frac{2(1+D^{*2})\alpha}{(\gamma+1)D^{*2}}\psi', \quad u_2' = (D_s^* - M_s^*)\mathrm{i}k\psi', \\ p' = -\frac{4\gamma M_s^*\alpha}{(\gamma+1)}\psi', \quad \lambda' = 0, \end{aligned}\right\} \tag{4.9}$$

so that

$$\boldsymbol{\zeta}(0) = \left[\frac{4\alpha}{(\gamma+1)D^{*2}M_s^*},\ \frac{2(1+D^{*2})\alpha}{(\gamma+1)D^{*2}},\ (D_s^* - M_s^*)\mathrm{i}k,\ -\frac{4\gamma M_s^*\alpha}{(\gamma+1)},\ 0\right]^{\mathrm{T}}. \tag{4.10}$$

Finally, a rear-boundary condition on the perturbations is applied at the equilibrium point of the steady detonation such that there are no acoustic waves propagating upstream. This leads to the acoustic radiation condition (Buckmaster & Ludford 1986)

$$\alpha u_1' - \mathrm{i}k u_{1b}^* u_2' - \frac{v_b^*}{\gamma c_b^*}\left[\alpha^2 + k^2 c_b^{*2}(1 - M_b^{*2})\right]^{1/2} p' = 0, \tag{4.11}$$

which in terms of $\boldsymbol{\zeta}$ can be written as

$$\left[0,\ \alpha,\ -\mathrm{i}k u_{1b}^*,\ -\frac{v_b^*}{\gamma c_b^*}\left[\alpha^2 + k^2 c_b^{*2}(1 - M_b^{*2})\right]^{1/2},\ 0\right]\cdot\boldsymbol{\zeta}(\infty) = 0, \tag{4.12}$$

where u_{1b}^*, v_b^*, c_b^* and M_b^* are the unperturbed longitudinal velocity, specific volume, isentropic sound speed and flow Mach number respectively in the burnt gas. This condition is applied at $x = \infty$, i.e. at the equilibrium point of the detonation for the present reaction model, where $\lambda^* \to 1$ in an exponential manner.

The stability equations (4.4) are solved by the implementation of the two-point boundary value solution technique described in Short (1997*a*), based upon that of Lee & Stewart (1990*a*). Starting from an initial guess for α, (4.4) are integrated from the detonation shock, with (4.10) as initial conditions, to the equilibrium point in the burnt zone. In practice, this is taken numerically at a point where the perturbation eigenfunctions associated with the exponentially decaying reaction progress variable in the burnt zone are negligibly small. A standard two-variable Newton–Raphson iteration is then employed on the acoustic radiation condition (4.12) to iterate on α until this condition is satisfied to within a specified tolerance.

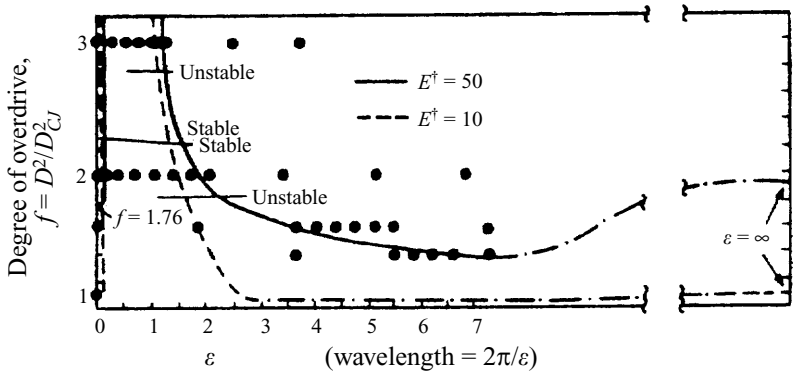

FIGURE 4. Neutral stability boundaries in f, k space obtained by Erpenbeck (1964) for $Q = 50$, $\gamma = 1.2$ and for $E = 10$ and $E = 50$, taken from Fickett & Davis (1979). In the figure, the parameter ϵ is equivalent to the wavenumber k used in the present study. Wavenumbers between the two solid lines are unstable for $E = 50$ and between the two dashed lines for $E = 10$.

5. Erpenbeck's linear stability results

Before presenting the results of the present analysis, it will be instructive to recall the relevant results of Erpenbeck (1964, 1965, 1966, 1970). Until now, these have represented the only major source of information regarding the calculation of two-dimensional neutral stability boundaries for varying detonation bifurcation parameters. In contrast to the normal-mode formulation used here, Erpenbeck treated the linear stability calculation as an initial value problem for infinitesimal perturbations of the steady-state flow, in which the perturbation time-dependence was treated by a Laplace transform analysis. By analysing the location of the pole singularities of the transform function for a given set of detonation parameters, stability or instability was established pointwise for a given transverse perturbation wavenumber k. This method is equivalent to a sampling of parameter space and meant that the neutral stability boundaries had to be inferred by interpolation. Moreover, for a given bifurcation problem, little or no information regarding the nature of the stability spectrum, for example the number of unstable modes, their growth rates, relative frequencies, spatial structure or phase and group velocity profiles was given.

Figure 4, from Fickett & Davis (1979), shows Erpenbeck's interpolated neutral stability boundaries in wavenumber space as the degree of overdrive is varied for the two activation energies $E = 10$ and $E = 50$ with $Q = 50$ and $\gamma = 1.2$. The dots indicate the locations at which pointwise stability or instability was determined. The region between the two solid lines is unstable for $E = 50$ and between the two dashed lines for $E = 10$. In both cases there is a finite-wavenumber band of instability which appears to persist as f is increased. In the following, it will be demonstrated that this feature is associated with the lowest frequency, fundamental unstable mode. In contrast, the unstable higher frequency modes that are present for lower f, and play a significant role in determining a more complex behaviour of the right-hand neutral stability boundary than that envisaged by Erpenbeck, are stabilized as the overdrive is increased. Erpenbeck (1964) also noted that an asymptotic analysis of the linear stability behaviour for very large f would be tractable, where the steady flow approaches that of a non-reactive step-shock, which, in the limit, is neutrally stable. Recently, Clavin & He (1996) have conducted a detonation stability analysis for longitudinal disturbances in this limit, but for a different reaction model to that considered by Erpenbeck (1964). The results shown below also illustrate that an

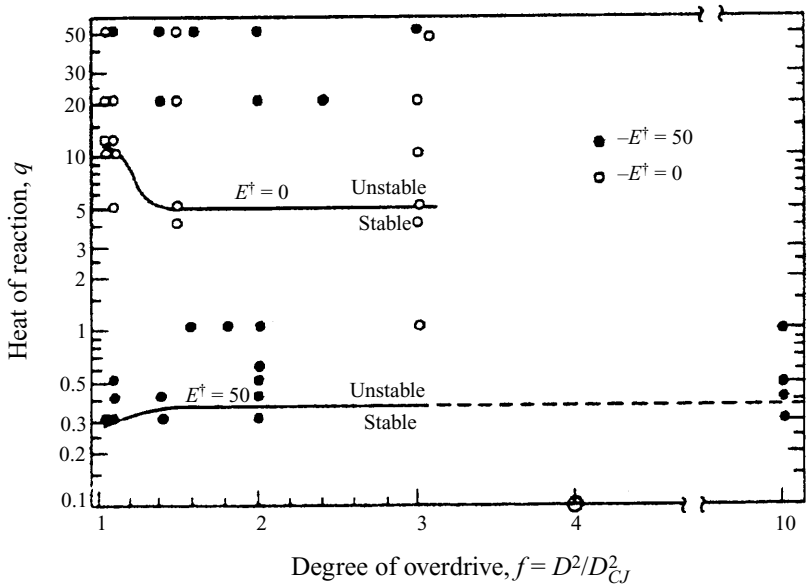

FIGURE 5. Neutral stability boundaries in Q verses f space obtained by Erpenbeck (1964, 1965, 1970) for $Q = 50$, $\gamma = 1.2$ and for $E = 0$ and $E = 50$. From Fickett & Davis (1979).

important understanding of the linear stability behaviour for the present one-step Arrhenius reaction model can be gained in situations when the overdrive is increased from its CJ value to moderately or highly overdriven values.

The chain-lines in figure 4 are an addition made by Fickett & Davis (1979) and represent a possible pathway of connection between the interpolated neutral stability curves and an asymptotic prediction of the small-wavelength stability for these parameters (Erpenbeck 1966). The analysis in Erpenbeck (1966) is valid for wavelengths long relative to a mean free path, but short relative to the characteristic detonation reaction zone width. The asymptotic criterion for short-wavelength stability was found to depend on the steady-state profiles of the quantity $c^{*2}\eta$, where η is the sonic parameter $1-u_1^{*2}/c^{*2}$. Detonations for which $c^{*2}\eta$ decreases monotonically are found to be stable. Stability in cases where this quantity increases either monotonically or up to a maximum is determined through the evaluation of simple integral functions of the steady flow variables. For both cases in figure 4, arbitrary short-wavelength instability is predicted as $k \to \infty$ for sufficiently low overdrives.

However, it will be shown below that in cases for which Erpenbeck (1966) predicts short-wavelength instability, our numerical calculations show that short-wavelength stability prevails. In fact, for all the calculations we perform, a high-wavenumber neutral stability is always present. Due to limitations on the numerical procedure used by Erpenbeck, short-wavelength numerical calculations were not carried out, and so the asymptotic results were not verified numerically. It is clear that the asymptotic scalings studied by Erpenbeck (1966) should be re-examined in the light of the present findings to establish the modifications required to explain the numerical results.

Figure 5 shows a summary from Fickett & Davis (1979) of the interpolated two-dimensional neutral stability boundaries in Q versus f space for the two activation energies $E = 50$ (Erpenbeck 1964) and $E = 0$ (Erpenbeck 1965). As before, the dots represent the locations where stability or instability was determined pointwise. The

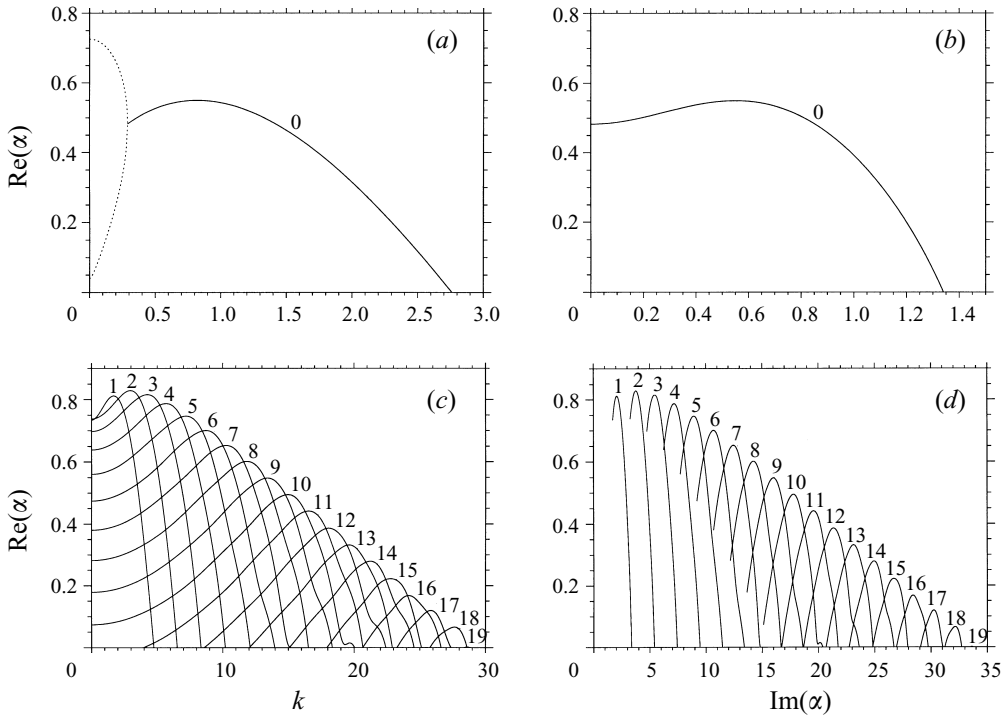

FIGURE 6. (*a*) Re(α) vs. k and (*b*) Re(α) vs. Im(α) for the lowest frequency two-dimensional unstable mode present when $Q = 50$, $E = 50$, $\gamma = 1.2$, $f = 1$. The dotted line in (*a*) indicates non-oscillatory modes. (*c*) Re(α) vs. k and (*d*) Re(α) vs. Im(α) for the 19 higher frequency two-dimensional unstable modes present when $Q = 50$, $E = 50$, $\gamma = 1.2$, $f = 1$.

results for $E = 0$, where the exponential sensitivity of the reaction rate to changes in the thermodynamic state is eliminated, demonstrate that instability can still occur providing the reaction is sufficiently exothermic. The case for $E = 50$ demonstrates that, in general, global two-dimensional detonation stability occurs only for very small heats of reaction. Erpenbeck (1964) noted that stability must occur as $Q \to 0$, since the steady detonation is then a step shock, which for a finite Mach number in a non-reactive, ideal gas is stable (see the Appendix).

Below we present results characteristic of the linear stability behaviour for systematic variations in the bifurcation parameters, the overdrive f, activation energies E or θ and heat releases Q or β, using, in contrast to Erpenbeck's formulation, the normal-mode procedure given in §4.

6. The normal-mode linear stability spectrum for two-dimensional detonation disturbances

6.1. *Stability behaviour for varying overdrive f*

Figure 6 shows the stability behaviour arising for a Chapman–Jouguet wave $f = 1$, with $\gamma = 1.2$, $Q = 50$ and $E = 50$ ($\beta = \theta = 10.39$). The spectrum consists of 20 two-dimensionally unstable modes. Figures 6(*a*) and 6(*b*) show the behaviour of the lowest frequency (fundamental) unstable mode, while figures 6(*c*) and 6(*d*) show the behaviour of the 19 higher frequency unstable modes. Here, and in the following, the unstable modes have been ordered, starting with the label 0 for the lowest frequency

or fundamental mode, according to their relative frequencies either at $k = 0$, or at the neutrally stable wavenumber above which the mode is unstable. The lowest frequency mode shown in figure 6(*a*) has two real components for $k < k_m = 0.29$, identifying a range of unstable non-propagating wavenumbers. A critical bifurcation point is reached at $k = k_m$ where the mode becomes oscillatory and disturbances with wavenumbers greater than k_m now travel transverse to the detonation front. For $k > k_m$, the growth rate of the oscillatory mode first increases with k, reaching a maximum at $\mathrm{Re}(\alpha) = 0.550$ at $k = 0.82$, before decaying and becoming dissipative for $k > 2.76$. The wavelength, defined as $W = 2\pi/k$, corresponding to the maximum growth rate of the oscillatory component is $W = 7.66$. For $k > k_m$, the frequency increases monotonically with increasing wavenumber.

The first ten higher frequency modes shown in figures 6(*c*) and 6(*d*) have positive growth rates at $k = 0$, i.e. are longitudinally unstable modes. Each of these unstable modes possesses the generic feature of a growth rate which increases monotonically with increasing k, before reaching a maximum. Further increases in k lead to a decay in the growth rate until a critical wavenumber is reached at which the mode becomes stable. The corresponding frequency of each mode increases monotonically with k. The largest growth rate $\mathrm{Re}(\alpha) = 0.829$ at $k = 2.96$ ($W = 2.12$) is associated with the second of the higher frequency modes. The final nine higher frequency unstable modes are all longitudinally stable, but increases in wavenumber lead to the presence of a finite band of two-dimensional instability. Each of these modes has an associated maximum growth rate, with that of the highest frequency unstable mode being $\mathrm{Re}(\alpha) = 0.002$ at $k = 28.57$ ($W = 0.220$). Above a value $k = 28.80$, our computations reveal that no further unstable modes are present, and thus there is a critical small perturbation wavelength $W = 0.218$, below which linear disturbances will not render the detonation unstable.

Given the large number of unstable linear modes, it is instructive to reflect both on the structure of the underlying steady detonation wave shown in figure 1, i.e. for $f = 1$, $\gamma = 1.2$, $Q = 50$ and $E = 50$, and the role that these 20 linearly unstable modes might play in the onset of cellular detonation. For this parameter set, the steady structure approaches that of a classical square-wave profile. In particular, the width of the main heat release layer, which we signify here and in the following as the region defined by $0.1 < \lambda < 0.95$, is given by $X = 0.65$. This is compared to the disturbance wavelength $W = 0.218$, below which the detonation is stable. With such complex stability behaviour, a random initial disturbance in a sufficiently wide channel will potentially excite a large range of transverse disturbances, with locally dominant growth around the wavelength associated with the maximum growth rate of each unstable mode. Although standard linear stability arguments predict that a transverse structure with a wavelength $W = 2.12$ will ultimately be the most dominant, at least initially the fact that several high-frequency linear modes could be excited nevertheless points to the emergence of an irregular cellular structure. An indication that this is the case is given in Bourlioux & Majda (1992), and is investigated in more detail with very high-resolution numerical simulations in wide channels by Quirk & Short (1998). On the other hand, such irregular structures have also been observed in experiments with either a low percentage of inert diluent (e.g. Strehlow 1970) or for an ambient atmosphere with a moderately large initial pressure. For the present detonation parameters, i.e. $f = 1$, $\gamma = 1.2$, $Q = 50$ and $E = 50$, the post-shock-scaled heat release $\beta = 10.39$ is moderately large. The complexity of the linear stability spectrum would thus appear to be consistent with the experimental results.

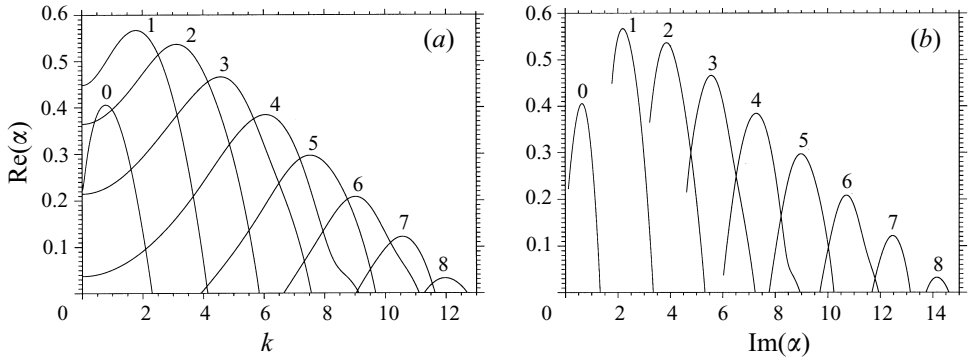

FIGURE 7. Stability spectrum showing (*a*) Re(α) vs. k and (*b*) Re(α) vs. Im(α) for the nine two-dimensional unstable modes when $Q = 50$, $E = 50$, $\gamma = 1.2$ and $f = 1.2$.

It is also interesting to remark on a particular correlation between linear stability behaviour and numerical simulations of one-dimensional pulsating detonation waves (Fickett & Wood 1966; Bourlioux *et al.* 1991; Short & Quirk 1997). In cases where a one-dimensional linear stability analysis reveals the presence of one or several higher frequency unstable modes in addition to the lowest frequency mode, long-time nonlinear calculations reveal a period of oscillation which closely approximates that associated with the lowest frequency linear mode. An analogous property for two-dimensional calculations would indicate that particular attention should then be focused on the lowest frequency two-dimensional mode where, for the present parameter set in figure 6, the maximum growth rate of the oscillatory component has an associated wavelength $W = 7.66$.

Figure 7 shows the change in the linear stability spectrum which results from increasing the overdrive to $f = 1.2$ with $E = 50$, $Q = 50$ and $\gamma = 1.2$ fixed. The corresponding values of β and θ are $\beta = \theta = 8.96$ There are nine modes of instability. The lowest frequency mode has no non-oscillatory growth. Only the first five modes are longitudinally unstable, while the four highest frequency modes are longitudinally stable. Thus the increase in overdrive from $f = 1$ to $f = 1.2$ along with the resulting decrease in β and θ has resulted in the suppression of the ten highest frequency unstable modes present for $f = 1$. Stability occurs for all disturbances with wavelengths $W < 0.50$, which is larger than the corresponding value $W < 0.218$ for $f = 1$. The fastest growing mode is now associated with the first higher frequency mode, having switched from the second higher frequency mode at $f = 1$, and having a maximum growth rate Re(α) = 0.567 at $k = 1.78$ ($W = 3.53$). Since this wavelength is longer than the corresponding wavelength $W = 2.12$ for $f = 1$, the result of an increase in f is that larger detonation cells are expect to emerge initially. On the other hand, there is a drop in the maximum growth rate from Re(α) = 0.829 at $f = 1$ to Re(α) = 0.567 at $f = 1.2$ and the instability evolution time scale is increased. The maximum growth rate of the lowest frequency unstable mode is given by Re(α) = 0.406 at $k = 0.78$ ($W = 8.03$).

Figure 8 shows the different characteristic behaviour of the perturbation eigenfunction structures $z'(x)$ corresponding to the points of the maximum growth rate of the lowest frequency unstable mode (0) at $k = 0.78$ ($W = 8.03$) and the highest frequency unstable mode (8) at $k = 11.95$ ($W = 0.53$). The eigenfunction structure relating to the lowest frequency mode is observed to be slowly varying in space, growing in amplitude through the main heat release layer but decaying into the equilibrium

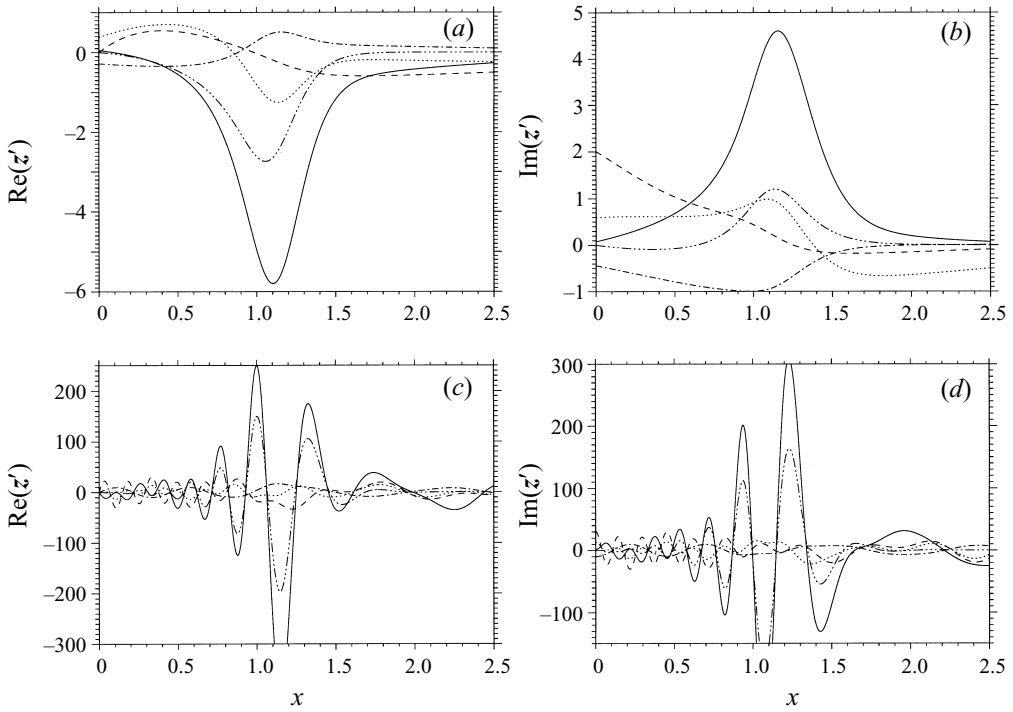

FIGURE 8. Perturbation eigenfunction structures showing (*a*) Re(z') vs. x and (*b*) Im(z') vs. x for the fundamental unstable mode (0) at the point of its maximum growth rate $k = 0.78$ ($W = 8.03$), (*c*) Re(z') vs. x and (*d*) Im(z') vs. x for the highest frequency unstable mode (8) at the point of its maximum growth rate $k = 11.95$ ($W = 0.53$) for $Q = 50$, $E = 50$, $\gamma = 1.2$ and $f = 1.2$. The curves correspond to v' (solid line), u_1' (dotted line), u_2' (dashed line), p' (dash-dot line) and Y' (dash-dot-dot-dot line).

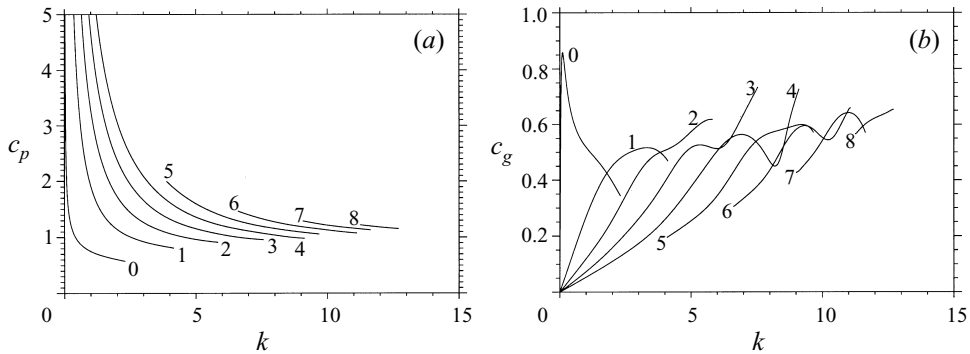

FIGURE 9. The variation of (*a*) the phase velocity $c_p = \mathrm{Im}(\alpha)/k$ and (*b*) the group velocity $c_g = \partial \mathrm{Im}(\alpha)/\partial k$ with wavenumber k for the unstable modes shown in figure 7.

zone. In contrast, the eigenfunction structure relating to the highest frequency mode varies rapidly in space, oscillating several times through the underlying steady wave structure, before again decaying into the equilibrium zone.

Figure 9 shows the behaviour of the phase velocities $c_p = \mathrm{Im}(\alpha)/k$ and group velocities $c_g = \partial \mathrm{Im}(\alpha)/\partial k$ of each of the unstable modes shown in figure 7. At a fixed wavenumber k, the largest phase velocity is associated with the highest frequency

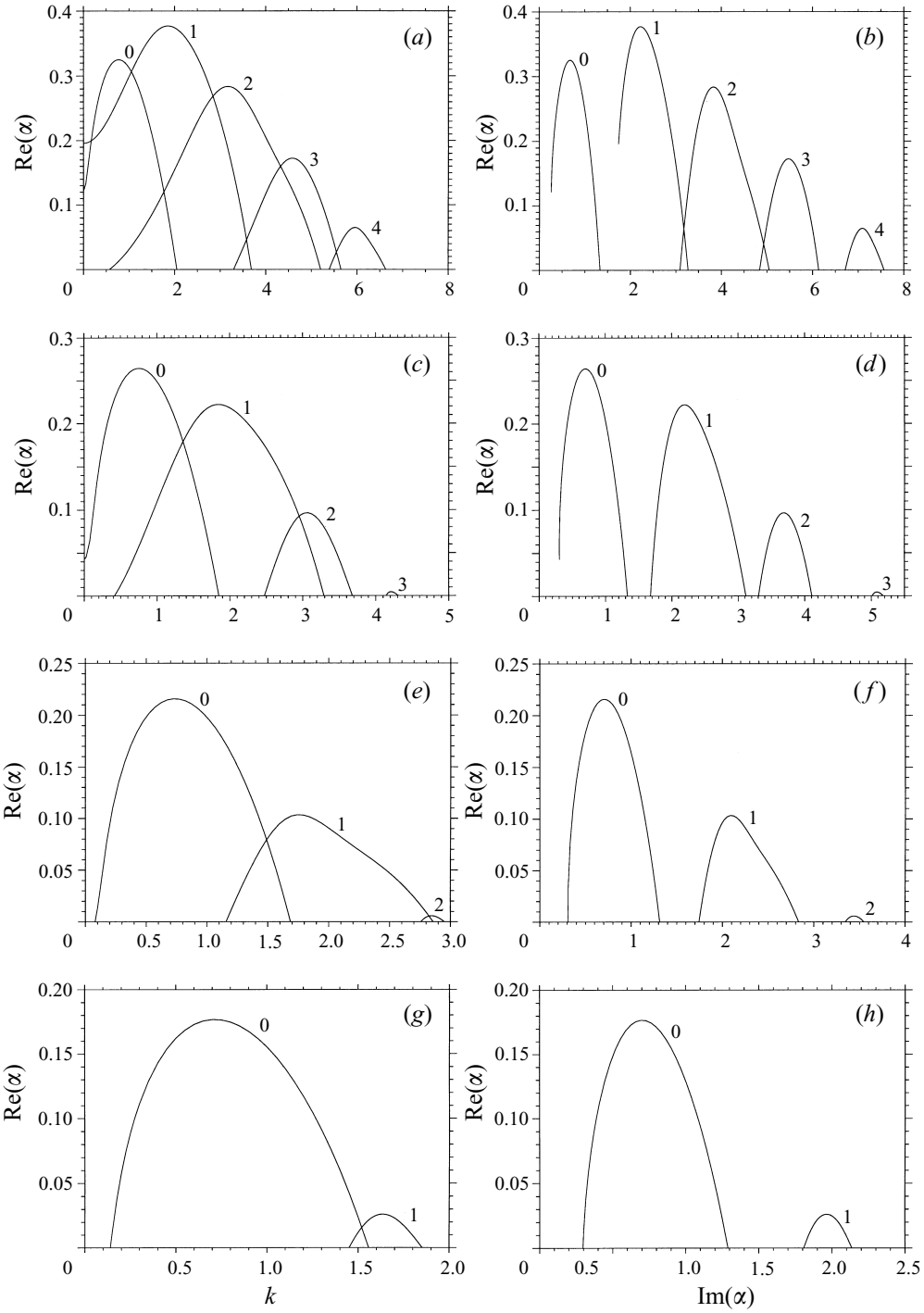

FIGURE 10. Stability spectrum showing (*a*) Re(α) vs. k and (*b*) Re(α) vs. Im(α) for the five two-dimensional unstable modes present when $Q = 50$, $E = 50$, $\gamma = 1.2$ and $f = 1.4$; (*c*) Re(α) vs. k and (*d*) Re(α) vs. Im(α) for the four two-dimensional unstable modes present when $Q = 50$, $E = 50$, $\gamma = 1.2$ and $f = 1.6$; (*e*) Re(α) vs. k and (*f*) Re(α) vs. Im(α) for the three two-dimensional unstable modes present when $Q = 50$, $E = 50$, $\gamma = 1.2$ and $f = 1.8$; (*g*) Re(α) vs. k and (*h*) Re(α) vs. Im(α) for the two two-dimensional unstable modes present when $Q = 50$, $E = 50$, $\gamma = 1.2$ and $f = 2.0$.

unstable mode for that wavenumber. The distribution of the group velocity, on the other hand, is considerably more complex. The maximum value attained is $c_g = 0.858$ at $k = 0.11$ ($W = 58.23$) and is associated with the lowest frequency mode (0). The role that the phase and group velocities of linearly unstable modes might play in the dynamics of cell formation has become an issue since the work of Yao & Stewart (1996). Their long-wavelength, slowly evolving, two-dimensional detonation evolution equation predicts long-time nonlinear cells with a wavelength corresponding to the low-wavenumber neutral stability boundary present in the linearized version of the equation. However, it is interesting to note that both the phase and group velocities corresponding to the linearized dispersion relation are also a maximum at this point. Further analysis is required to understand the physical mechanisms of this selection within the context of a nonlinear evolution equation for cellular instability and the role, if any, of the phase and group velocity then established.

Figure 10 shows the change in the stability spectrum which results from increasing the overdrive from $f = 1.2$ through the values $f = 1.4$, $f = 1.6$, $f = 1.8$ to $f = 2.0$ with $E = 50$, $Q = 50$ and $\gamma = 1.2$ fixed. The corresponding values of β and θ are $\beta = \theta = 7.88$ for $f = 1.4$, $\beta = \theta = 7.03$ for $f = 1.6$, $\beta = \theta = 6.35$ for $f = 1.8$ and $\beta = \theta = 5.78$ for $f = 2.0$. An increase in overdrive f for fixed Q, E and γ, thus corresponds to a decrease in β and θ and consequently a less thermodynamically sensitive reaction process behind the detonation shock. The increase in overdrive from $f = 1.2$ to $f = 1.4$ suppresses the four highest frequency modes present at $f = 1.2$. The maximum growth rate is still governed by the first higher frequency mode, but has now dropped to $\mathrm{Re}(\alpha) = 0.377$ at $k = 1.85$ ($W = 3.40$). At $f = 1.4$, the steady wave is stable to all disturbances with $W < 0.95$. An overdrive increase to $f = 1.6$ suppresses one further higher frequency mode, leaving only four unstable modes, but the lowest frequency mode now determines the global maximum growth rate $\mathrm{Re}(\alpha) = 0.264$ at $k = 0.77$ ($W = 8.16$). At this stage, only the lowest frequency mode is unstable to one-dimensional disturbances. The range of unstable wavelengths $W > 1.46$ has also decreased. A further increase in overdrive to $f = 1.8$ suppresses an additional higher frequency unstable mode, leaving only three unstable modes. The maximum growth rate is determined by the lowest frequency mode having $\mathrm{Re}(\alpha) = 0.216$ at $k = 0.72$ ($W = 8.70$). At $f = 1.8$, there is only a finite wavenumber band of two-dimensional instability for $2.13 < W < 79.19$, the lowest frequency mode having crossed the neutral stability boundary $f = 1.731$ (Lee & Stewart 1990*a*) for one-dimensional instability. At $f = 2.0$, there is a single low-frequency mode, with maximum growth rate $\mathrm{Re}(\alpha) = 0.177$ at $k = 0.70$ ($W = 8.96$), and a single higher frequency mode present. Disturbances with $W < 3.39$ are short-wavelength stable for $f = 2.0$. Thus as f increases, the wavelength corresponding to the maximum global growth rate also increases, and standard linear stability arguments point to the initial evolution of ever larger detonation cells in an unstable flow. In line with the suppression of the higher frequency linear modes as f increases from $f = 1.0$ to $f = 2.0$, the corresponding steady detonation wave structure (figure 1) is observed to lose its square-wave nature. A broader main heat release layer develops, with the layer $0.1 < \lambda < 0.95$ having a width $X = 1.21$ at $f = 1.4$, while at $f = 1.8$ the same layer has width $X = 1.75$. There are marked decreases in both the pressure drop through the main heat release layer as β decreases and the peak of reaction rate as β and θ decrease.

As the overdrive is increased above $f = 2.19$, all previous higher frequency unstable modes are suppressed and the low-frequency mode emerges as the single unstable root. The behaviour of this mode for $f = 2.2$ ($\beta = \theta = 5.31$) is shown in figure 11. It is stable to longitudinal disturbances, has a low-wavenumber neutral stability point at

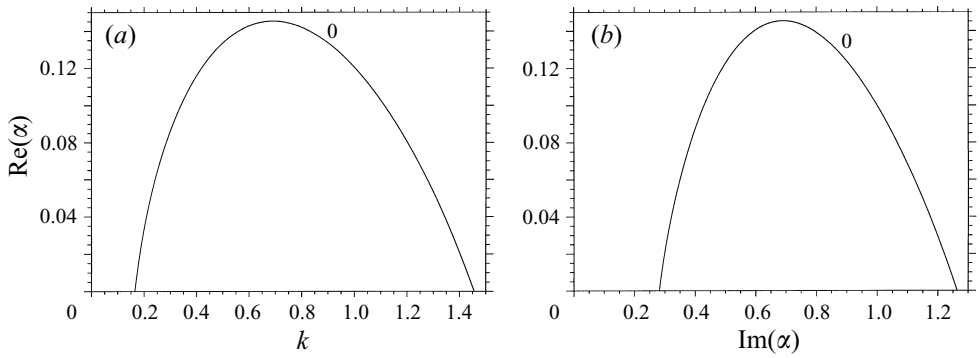

FIGURE 11. Stability spectrum showing (*a*) Re(α) vs. k and (*b*) Re(α) vs. Im(α) for the one two-dimensional unstable mode with $Q = 50$, $E = 50$, $\gamma = 1.2$ and $f = 2.2$.

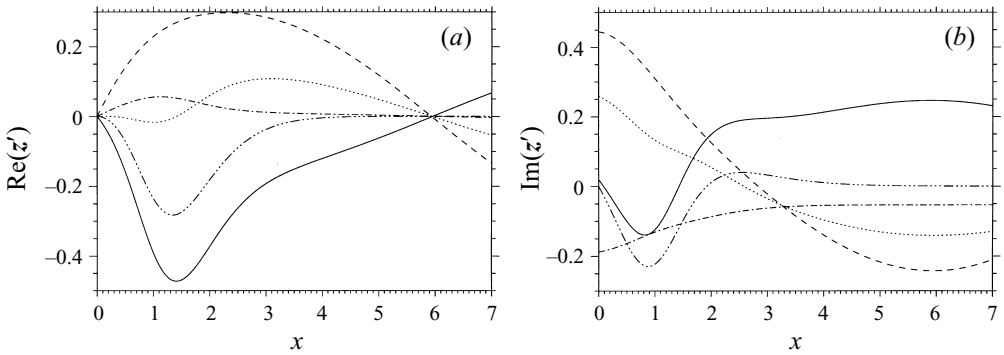

FIGURE 12. Perturbation eigenfunction structure showing (*a*) Re(z') vs. x and (*b*) Im(z') vs. x at the low-wavenumber neutral stability point $k = 0.16$ for the single unstable mode when $Q = 50$, $E = 50$, $\gamma = 1.2$ and $f = 2.2$. The curves correspond to v' (solid line), u_1' (dotted line), u_2' (dashed line), p' (dash-dot line) and Y' (dash-dot-dot-dot line).

$k = 0.16$ ($W = 38.13$), a maximum growth rate Re(α) = 0.145 at $k = 0.69$ ($W = 9.15$) and is stable for wavenumbers $k > 1.46$ ($W < 4.31$). The corresponding frequency at the low-wavenumber neutral stability point is Im(α) = 0.282 and at the high-wavenumber point, Im(α) = 1.263. Figures 12, 13 and 14 illustrate the difference in the perturbation eigenfunction structures at the three critical wavenumbers $k = 0.16$, $k = 0.69$ and $k = 1.46$. For comparison, the extent of the main heat release layer $0.1 < \lambda < 0.95$ in the corresponding steady wave structure for $f = 2.2$ is $X = 2.2$. Figure 12 illustrates the slowly varying nature of the perturbation eigenfunctions on this scale at the low-wavenumber point of neutral stability $k = 0.16$, for which further increases in k lead to instability. The more rapidly varying eigenfunction structures at the point of the maximum growth rate $k = 0.69$ are revealed in figure 13. In contrast to the slowly varying structures that initially lead to instability, figure 14 shows perturbation structures with oscillations on the spatial scale of main heat release at the high-wavenumber neutral stability point $k = 1.46$. Figure 15 shows the corresponding variation in the phase velocity c_p and group velocity c_g with wavenumber k for the single unstable root shown in figure 11. The low-wavenumber modes travel with a faster phase velocity than the high-wavenumber modes, with the largest phase velocity $c_p = 1.710$ at the low-wavenumber neutral stability point.

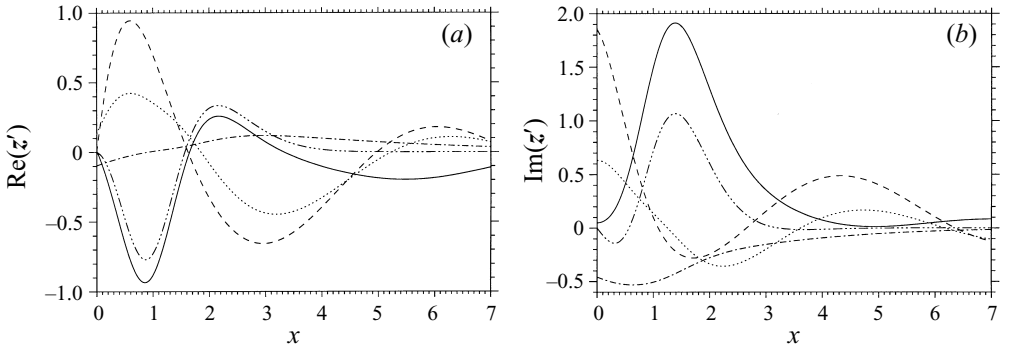

FIGURE 13. Perturbation eigenfunction structure showing (*a*) Re(z') vs. x and (*b*) Im(z') vs. x at the point of maximum growth rate for the single unstable mode $k = 0.69$ when $Q = 50$, $E = 50$, $\gamma = 1.2$ and $f = 2.2$. The curves correspond to v' (solid line), u_1' (dotted line), u_2' (dashed line), p' (dash-dot line) and Y' (dash-dot-dot-dot line).

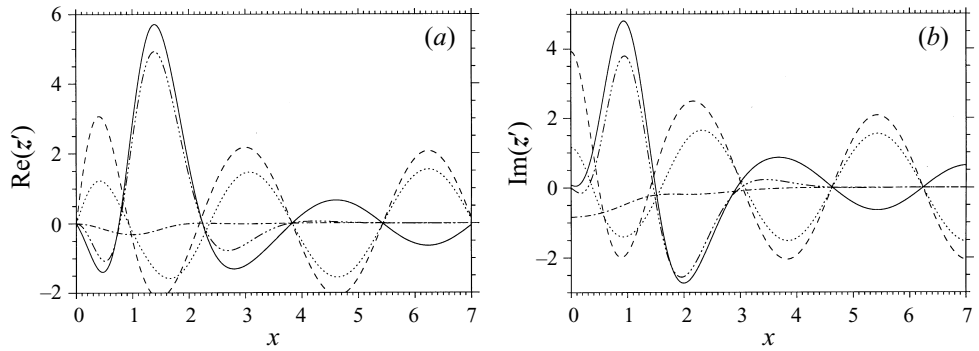

FIGURE 14. Perturbation eigenfunction structure showing (*a*) Re(z') vs. x and (*b*) Im(z') vs. x at the high-wavenumber neutral stability point $k = 1.46$ for the single unstable mode when $Q = 50$, $E = 50$, $\gamma = 1.2$ and $f = 2.2$. The curves correspond to v' (solid line), u_1' (dotted line), u_2' (dashed line), p' (dash-dot line) and Y' (dash-dot-dot-dot line).

The group velocity has a maximum $c_g = 0.895$ at $k = 0.19$, slightly shifted from the low-wavenumber neutral stability point.

With only a single mode of instability present, standard stability arguments imply that a transverse disturbance with wavelength $W = 9.15$ corresponding to the maximum growth rate $\mathrm{Re}(\alpha) = 0.145$ will emerge as the dominant linear feature. Numercial simulations (Bourlioux & Majda 1992; Quirk 1994) appear to show that regular detonation cells do indeed emerge when the stability behaviour is of the simple type found in figure 11. In experiments conducted in rectangular channels, regular cells are observed to form either in mixtures with a large percentage of inert diluent or for a low initial pressure of the ambient atmosphere. The present results, which show simple single-mode instability behaviour for large overdrives corresponding to a large post-shock temperature in the steady wave and thus comparatively low values of the post-shock scaled heat release β and activation energy θ, are again consistent with these observations.

Figure 16 shows the behaviour of the two neutral stability curves governing the lowest frequency, fundamental unstable mode as the overdrive is varied. For $f < 1.731$, the mode is longitudinally stable. The mode is always stable for a sufficiently large

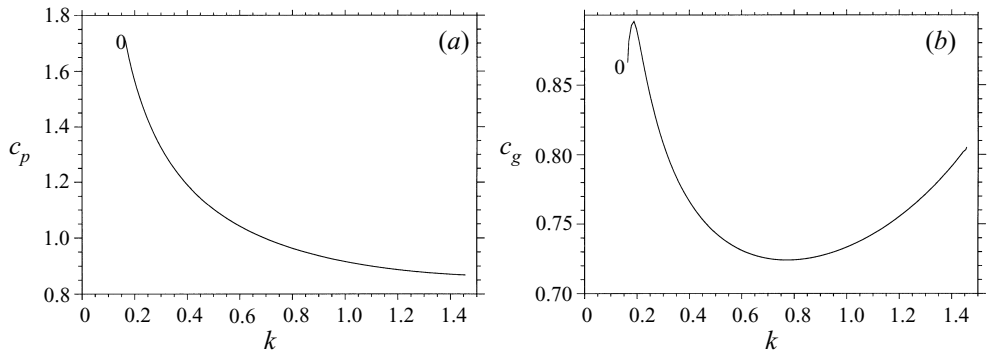

FIGURE 15. The behaviour of (*a*) the phase velocity $c_p = \mathrm{Im}(\alpha)/k$ and (*b*) the group velocity $c_g = \partial \mathrm{Im}(\alpha)/\partial k$ with wavenumber k for the mode shown in figure 11.

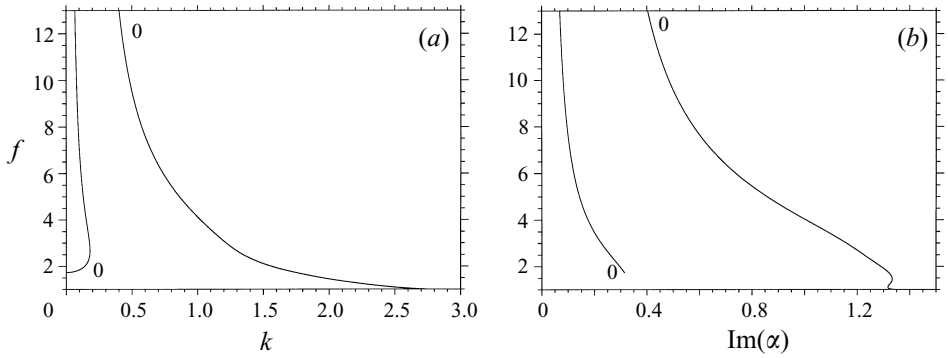

FIGURE 16. Neutral stability curves for varying overdrive f showing (*a*) f vs. k and (*b*) f vs. $\mathrm{Im}(\alpha)$ for the lowest frequency linear mode when $Q = 50$, $E = 50$, $\gamma = 1.2$. The region between the two curves in (*a*) is unstable.

wavenumber k, regardless of the overdrive. The band of unstable wavenumbers decreases for increasing f, but does not decrease to zero over the calculated range of f. At $f = 13$, the finite band of unstable wavelengths is $15.06 < W < 93.19$. The feature of instability at large values of f is in agreement with Erpenbeck (1964), and is explained by noting that the slowly varying nature of perturbation eigenfunction structures, characteristic of the transition to instability at the low-wavenumber neutral stability boundary, is unaffected by the increase in spatial scale characterizing the width of the steady detonation wave (figure 1), or main heat release layer, as f increases.

Figure 17 shows the behaviour of the sequence of neutral stability curves relating to the nine unstable modes present for $f = 1.2$ as the overdrive is varied. There are eleven additional higher frequency modes, whose neutral stability curves are not shown here, that are unstable at $f = 1$. As the overdrive is increased, each higher frequency mode reaches a critical bifurcation point above which it becomes stable, with the highest frequency unstable mode being the next to decay as f increases. For $f > 2.19$, only the lowest frequency unstable mode remains. Figure 18 shows the neutral stability boundary for $f \geqslant 1.2$ found from the union of the neutral stability curves shown in figure 17 which, for a particular f, determine the largest wavenumber region of instability. The left-hand boundary is that associated with the lowest frequency mode shown in figure 16. The right-hand boundary is of more interest since for $f < 2.19$

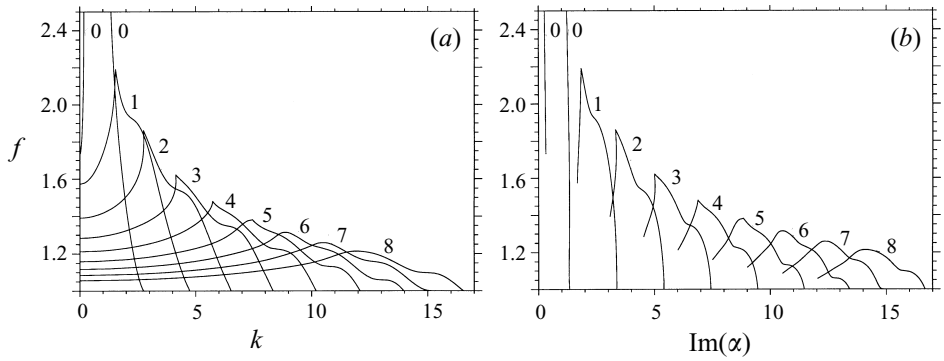

FIGURE 17. Neutral stability curves for varying overdrive f showing (a) f vs. k and (b) f vs. Im(α) for the lowest frequency linear mode and the eight higher frequency linear modes that are unstable at $f = 1.2$ when $Q = 50$, $E = 50$, $\gamma = 1.2$.

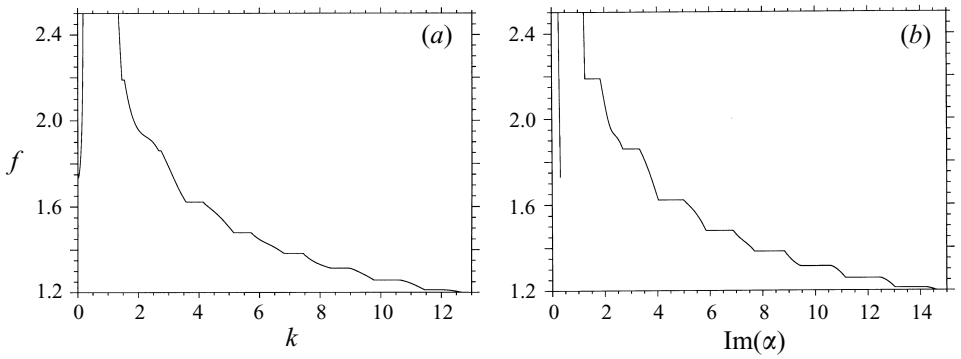

FIGURE 18. The two-dimensional neutral stability boundary for $f \geqslant 1.2$ showing (a) f vs. k and (b) f vs. Im(α) when $Q = 50$, $E = 50$ and $\gamma = 1.2$. The region between the two curves in (a) is unstable.

it consists of a sequence of discontinuous jumps. These result when a particular higher frequency mode reaches its stability bifurcation point and the mapping of the neutral stability boundary is then governed by a neighbouring unstable mode. Thus the actual neutral stability boundary in f versus k space for $Q = 50$, $E = 50$ and $\gamma = 1.2$ is markedly more complex than predicted by Erpenbeck (figure 4). Figures 16, 17 and 18 also emphasize the property that for all overdrives a right-hand, high-wavenumber, neutral stability boundary exists. The analysis undertaken by Erpenbeck (1966) predicts arbitrary short-wavelength instability for $f < 1.92$ when $Q = 50$, $E = 50$ and $\gamma = 1.2$, in contrast to the numerical results obtained here. The implication of the present results is that no two-dimensional instability is expected to develop in sufficiently narrow channels, and indeed this property has been observed experimentally (Strehlow & Crooker 1974).

In summary, we have found that increases in detonation overdrive lead to the sequential suppression of the higher frequency modes of instability. In contrast, the single lowest frequency mode of instability persists for large overdrives. The mode which governs the global maximum growth rate switches from the higher frequency modes to the lowest frequency mode, while the amplitude of the maximum growth rate also decreases as f increases. The range of wavelengths which render the steady detonation unstable is shortened as f increases, and for sufficiently large f, there is

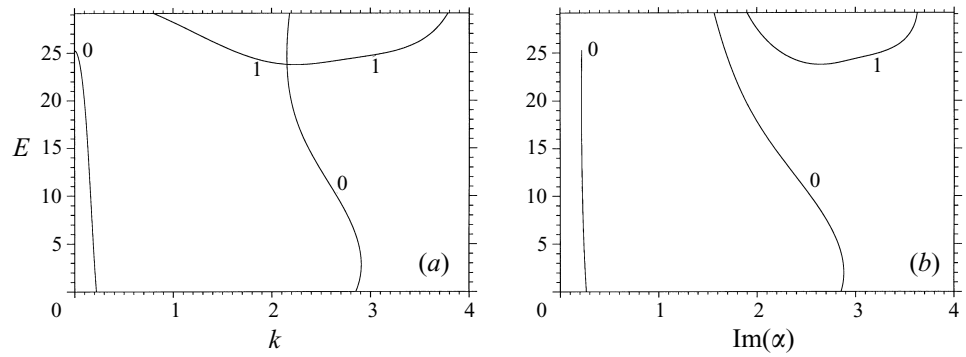

FIGURE 19. Neutral stability curves showing (*a*) E vs. k and (*b*) E vs. Im(α) for the two unstable modes present for $E < 29.13$ when $Q = 50$, $\gamma = 1.2$ and $f = 1.0$.

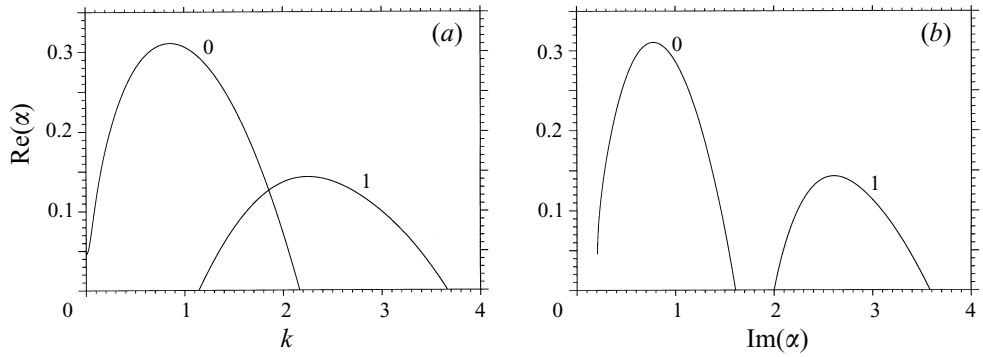

FIGURE 20. Stability behaviour showing (*a*) Re(α) vs. k and (*b*) Re(α) vs. Im(α) for the two two-dimensional unstable modes when $E = 27.5$, $Q = 50$, $\gamma = 1.2$ and $f = 1.0$.

only a finite band of two-dimensional instability, the one-dimensional instability being suppressed (Lee & Stewart 1990*a*). The structure of the perturbation eigenfunctions over the finite range of unstable wavenumbers for each mode also reveals a marked contrast in the characteristic spatial scale of their variations, as shown in figures 8, 12, 13 and 14.

6.2. *Stability behaviour for varying activation energy E*

Figures 19 to 24 show the behaviour of the linear stability spectrum with the activation energy E or θ as the bifurcation parameter. As the activation energy decreases, the steady wave structure and main heat release layer, described in §3.2, become longer, while the peak of the maximum reaction rate decreases as the exponential sensitivity of the reaction rate on local thermodynamic variations is weakened. The equilibrium state is identical for all E or θ. Figure 19 shows the neutral stability curves in E, k space for the one low-frequency and one higher frequency unstable mode present for $E < 29.13$ ($\theta < 6.05$) for a Chapman–Jouguet detonation $f = 1$, with $Q = 50$ and $\gamma = 1.2$. At $E = 29.13$, a second higher frequency unstable mode appears. For $E < 23.76$ ($\theta = 4.94$), the higher frequency mode is suppressed leaving only a single low-frequency mode of instability. For $E < 25.26$ ($\theta = 5.25$), the low-frequency mode is stable to longitudinal disturbances, but a finite band of unstable wavenumbers persists to $E = 0$ ($\theta = 0$). Instability is thus possible even when the exponential sensitivity of the reaction rate to fluctuations in the thermodynamic state is removed.

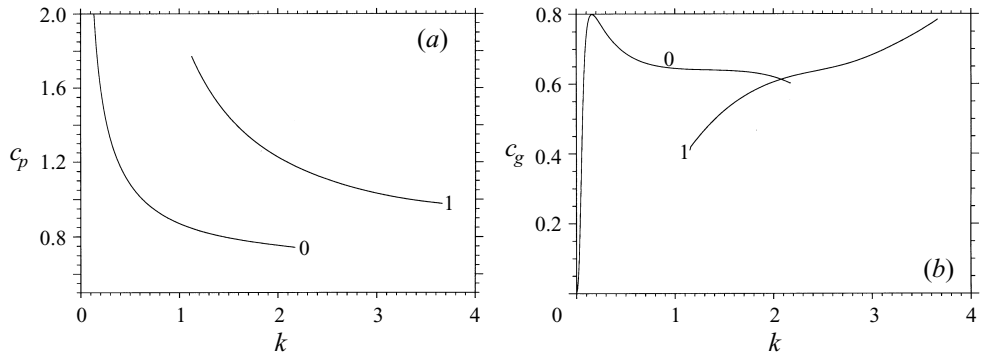

FIGURE 21. The behaviour of (*a*) the phase velocity $c_p = \mathrm{Im}(\alpha)/k$ and (*b*) the group velocity $c_g = \partial \mathrm{Im}(\alpha)/\partial k$ with wavenumber k for the two modes shown in figure 20.

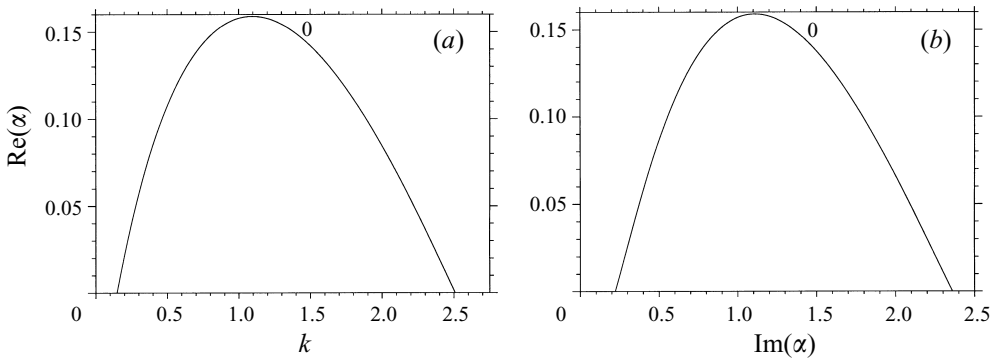

FIGURE 22. Stability behaviour showing (*a*) Re(α) vs. k and (*b*) Re(α) vs. Im(α) for the one two-dimensional unstable mode when $E = 12.5$, $Q = 50$, $\gamma = 1.2$ and $f = 1.0$.

The effect of exothermicity is sufficient to cause instability in such cases, confirming the result of Erpenbeck (1965). As in the case of increasing overdrive, it is the low-frequency fundamental mode that persists, the higher frequency modes being damped as the activation energy is decreased. Again we note the presence of a short-wavelength neutral stability boundary for all E shown.

Figure 20 shows the unstable k-spectrum for $E = 27.5$, $Q = 50$, $\gamma = 1.2$ and $f = 1$ ($\beta = 10.39$, $\theta = 5.71$). There are two unstable modes, with the maximum growth rate associated with the lowest frequency mode having $\mathrm{Re}(\alpha) = 0.310$ at $k = 0.86$ ($W = 7.35$). The lowest frequency mode is one-dimensionally unstable, while the higher frequency mode has the finite band of unstable wavenumbers, $1.71 < W < 5.56$. The detonation is stable to disturbances with wavelengths $W < 1.71$. The corresponding phase and group velocities of the two unstable modes are shown in figure 21. The maximum group velocity is associated with the lowest frequency mode, having $c_g = 0.799$ at $k = 0.16$ ($W = 39.23$).

Figure 22 shows the k-spectrum of the single low-frequency unstable mode present for $E = 12.5$, $Q = 50$, $\gamma = 1.2$ and $f = 1$ ($\beta = 10.39$, $\theta = 2.60$). The mode is one-dimensionally stable, having a low-wavenumber neutral stability point at $k = 0.15$ ($W = 42.36$). It attains a maximum growth rate $\mathrm{Re}(\alpha) = 0.159$ at $k = 1.10$ ($W = 5.74$), and is short-wavelength stable for $k > 2.51$ ($W < 2.51$). The slowly varying nature of the perturbation eigenfunctions $z'(x)$ at the low-wavenumber neutral stability point

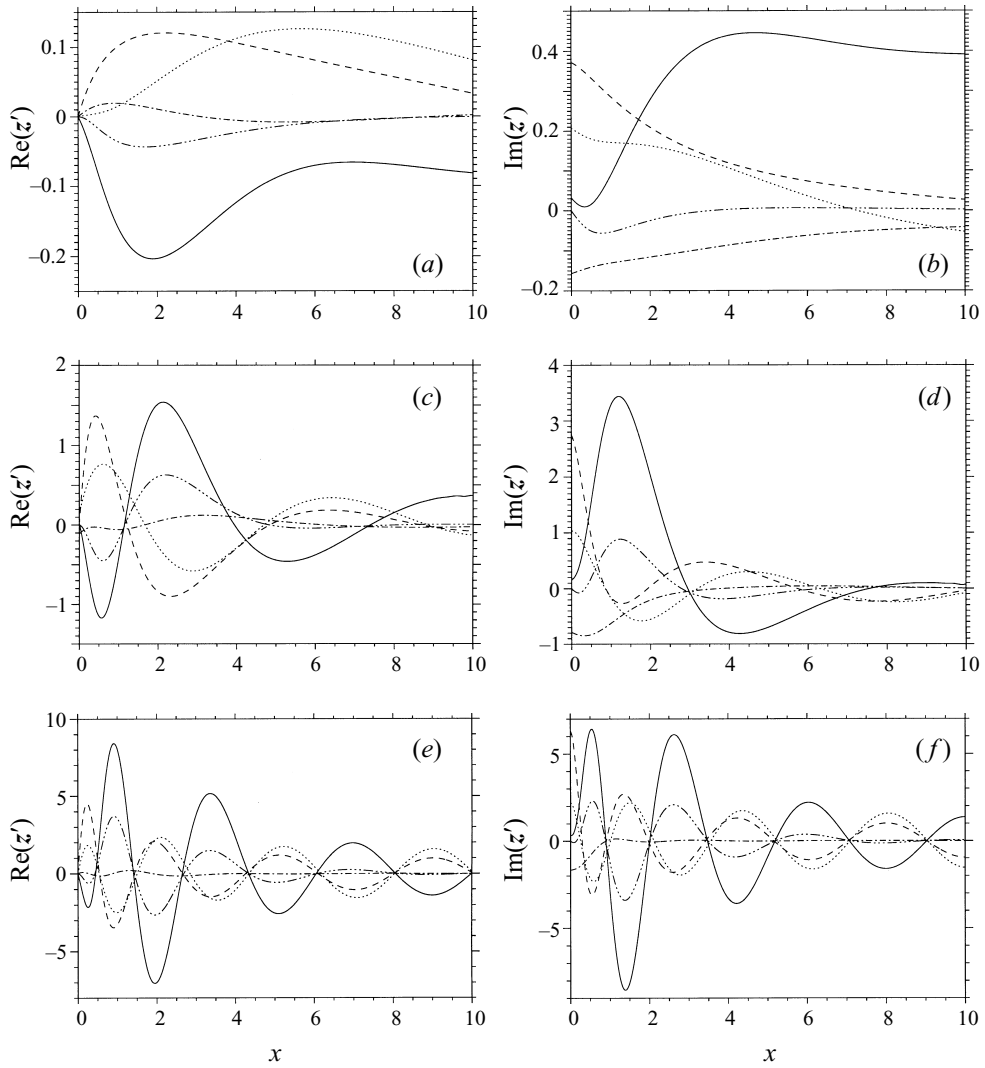

FIGURE 23. Perturbation eigenfunction structure showing (*a*) Re(z') vs. x and (*b*) Im(z') vs. x at the low-wavenumber neutral stability point $k = 0.15$, (*c*) Re(z') vs. x and (*d*) Im(z') vs. x at the point of maximum growth rate $k = 1.10$, (*e*) Re(z') vs. x and (*f*) Im(z') vs. x at the high-wavenumber neutral stability point $k = 2.51$ for the single unstable mode when $Q = 50$, $E = 12.5$, $\gamma = 1.2$ and $f = 1.0$. The curves correspond to v' (solid line), u_1' (dotted line), u_2' (dashed line), p' (dash-dot line) and Y' (dash-dot-dot-dot line).

$k = 0.15$ on the spatial scale $X = 7.10$ of the main heat release layer, determined by the region $0.1 < \lambda < 0.95$ in the steady wave, is again revealed in figures 23(*a*) and 23(*b*); that associated with the point of the maximum growth rate $k = 0.159$ is shown in figures 23(*c*) and 23(*d*). The rapidly varying perturbation eigenfunction behaviour associated with the high-wavenumber neutral stability point on the spatial scale of the main heat release layer $X = 7.10$ is shown in figures 23(*e*) and 23(*f*). The corresponding phase and group velocities for the single unstable mode at $E = 12.5$, $Q = 50$, $\gamma = 1.2$ and $f = 1$ are shown in figure 24. Both the maximum phase and group velocities occur at the low-wavenumber neutral stability point $k = 0.15$ ($W = 42.36$).

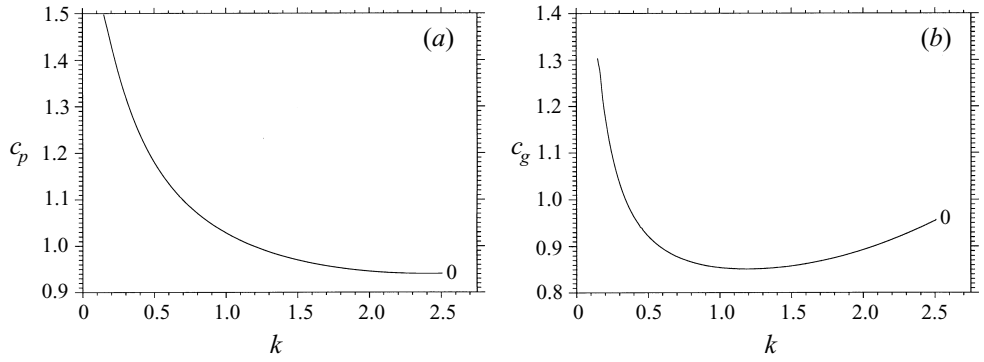

FIGURE 24. The behaviour of (*a*) the phase velocity $c_p = \mathrm{Im}(\alpha)/k$ and (*b*) the group velocity $c_g = \partial \mathrm{Im}(\alpha)/\partial k$ with wavenumber k for the mode shown in figure 22.

In summary, the effect on the linear stability response as the activation energy is decreased is qualitatively similar to that brought about by increases in the overdrive, since both limits quantitatively correspond to a decrease in the post-shock activation energy θ. It has also been established that the limits $f \gg 1$ or $E \ll 1$ for fixed Q and γ are insufficient in themselves to render the detonation stable to two-dimensional linear disturbances.

6.3. *Stability behaviour for varying heat release Q*

The detonation stability response with the heat of reaction Q as the bifurcation parameter is of interest both for the corresponding behaviour of the steady wave structure as Q decreases and for the inert-step-shock profile adopted in the limit $Q = 0$. As Q decreases for a fixed overdrive f, θ increases and the main heat release layer in the steady wave becomes thinner. Regimes of increasing instability should thus be encountered for decreasing Q. On the other hand, as $Q \to 0$ there is a decoupling in the feedback between the exothermic reaction and the hydrodynamic evolution of the system, and at $Q = 0$ the steady structure is an inert-Euler step shock. The relevant results on step-shock stability for an ideal gas are given in the Appendix, which shows that for finite propagation Mach numbers the shock is stable to linear perturbations. Thus in the limit $Q \to 0$, the detonation must become stable to two-dimensional linear perturbations (Erpenbeck 1964). However, the nature of the transition regime involving small but finite values of Q remains to be determined, and as discussed in §3.3, could in principle be investigated analytically based on the assumption of certain ordered limits between the post-shock-scaled activation energy θ and heat release β. This regime is of importance since a large proportion of the experiments on regular cellular detonation propagation are conducted in mixtures with a large percentage of inert diluent, i.e. in a low heat release system (Strehlow 1970; Lee 1984).

Figure 25 shows the behaviour of the neutral stability curves relating to the lowest frequency and first two higher frequency unstable modes present when $Q = 50$, $E = 50$, $\gamma = 1.2$ and $f = 1.2$ ($\beta = \theta = 8.96$) in the regime $1 \leqslant Q \leqslant 50$ ($0.815 < \beta < 8.96$, $8.96 < \theta < 40.75$). In this range, all three modes are one-dimensionally unstable. The band of unstable wavenumbers for each mode increases as Q decreases until small-Q regimes are reached, where an abrupt change in the stability spectrum can be noted. The increased range of instability for each of the modes is consistent with the underlying changes in the steady wave as Q decreases. The behaviour of the

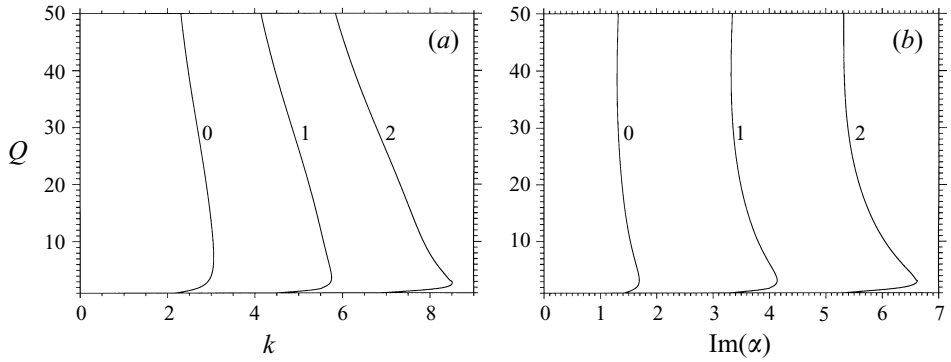

FIGURE 25. Neutral stability curves showing (*a*) Q vs. k and (*b*) Q vs. Im(α) for the lowest frequency mode and first two higher frequency modes that are unstable for $Q = 50$, $E = 50$, $\gamma = 1.2$ and $f = 1.2$.

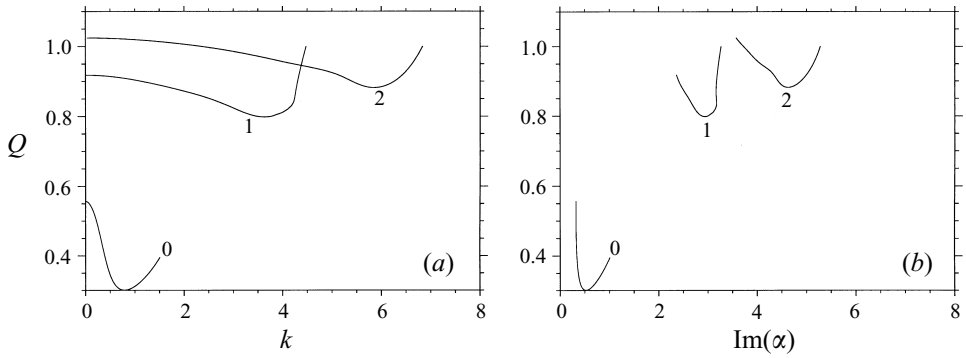

FIGURE 26. Neutral stability curves near $Q = 0$ showing (*a*) Q vs. k and (*b*) Q vs. Im(α) for the three modes shown in figure 25.

three modes near $Q = 0$ is shown in figure 26. As predicted from the known stability behaviour at $Q = 0$, each curve has a local minimum in Q, k space corresponding to a critical heat release below which the mode is stable. The second higher frequency mode is the first to be suppressed at $Q = 0.882$ ($\beta = 0.727$, $\theta = 41.23$), while the first higher frequency mode is stable for $Q < 0.798$ ($\beta = 0.664$, $\theta = 41.59$), and the lowest frequency mode is stable for $Q < 0.3$ ($\beta = 0.266$, $\theta = 44.26$).

The k-spectrum of the low-frequency unstable mode for $Q = 0.4$ ($\beta = 0.349$, $\theta = 43.62$) is shown in figure 27. The mode becomes unstable at $k = 0.39$ ($W = 16.32$), reaches a maximum growth rate Re(α) $= 0.032$ at $k = 0.78$ ($W = 8.11$) and has a high-wavenumber neutral stability point at $k = 1.53$ ($W = 4.11$). The small value of the maximum growth rate indicates the close proximity to a neutral stability boundary. The spatial behaviour of the perturbation eigenfunctions corresponding to the point of the maximum growth rate $k = 0.78$ for the low-frequency mode at $Q = 0.4$ is shown in figure 28. The corresponding phase and group velocities for this mode are shown in figure 29. It is interesting to note that while the phase velocity has a maximum at the low-wavenumber neutral stability point, the group velocity has a maximum at the high-wavenumber neutral stability point, in contrast to the examples shown previously.

Of relevance to the experimental literature is the construction and behaviour of a

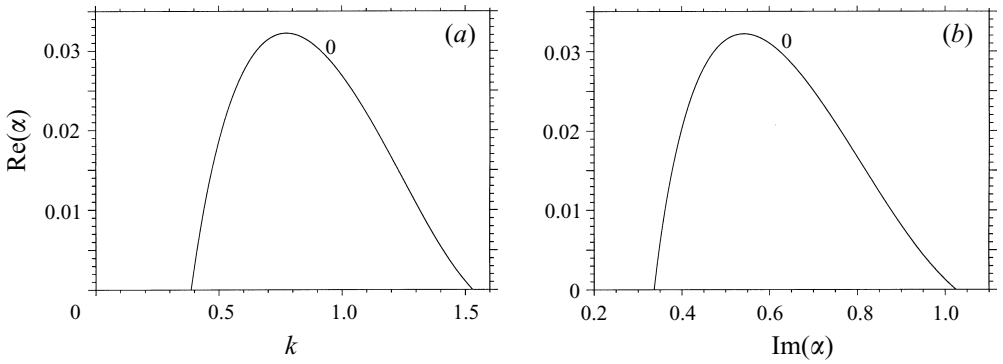

FIGURE 27. Stability behaviour showing (*a*) Re(α) vs. k and (*b*) Re(α) vs. Im(α) for the low-frequency mode at $Q = 0.4$, $E = 50$, $\gamma = 1.2$ and $f = 1.2$.

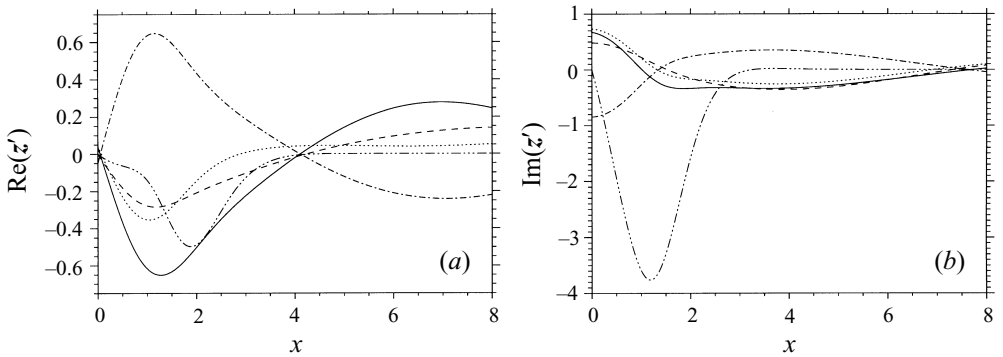

FIGURE 28. Perturbation eigenfunction structure showing (*a*) Re(z') vs. x and (*b*) Im(z') vs. x at the point of the maximum growth rate $k = 0.78$ for the low-frequency mode when $Q = 0.4$, $E = 50$, $\gamma = 1.2$ and $f = 2.2$. The curves correspond to v' (solid line), u_1' (dotted line), u_2' (dashed line), p' (dash-dot line) and Y' (dash-dot-dot-dot line).

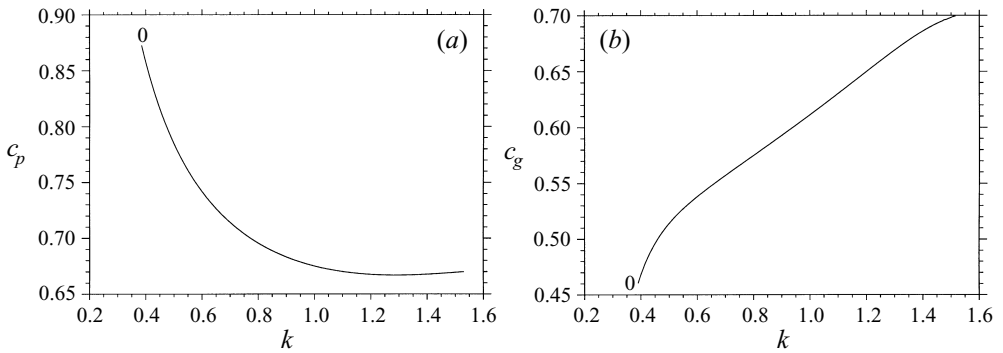

FIGURE 29. The behaviour of (*a*) the phase velocity $c_p = \mathrm{Im}(\alpha)/k$ and (*b*) the group velocity $c_g = \partial \mathrm{Im}(\alpha)/\partial k$ with wavenumber k for the mode shown in figure 27.

Q, E neutral stability diagram. Figure 30 shows the behaviour of the neutral stability curves for the lowest frequency modes near a minimum in Q, k space for the five activation energies $E = 0$, $E = 5$, $E = 10$, $E = 25$ and $E = 50$ when $\gamma = 1.2$ and $f = 1.2$. The circles indicate the value of Q below which stability prevails for

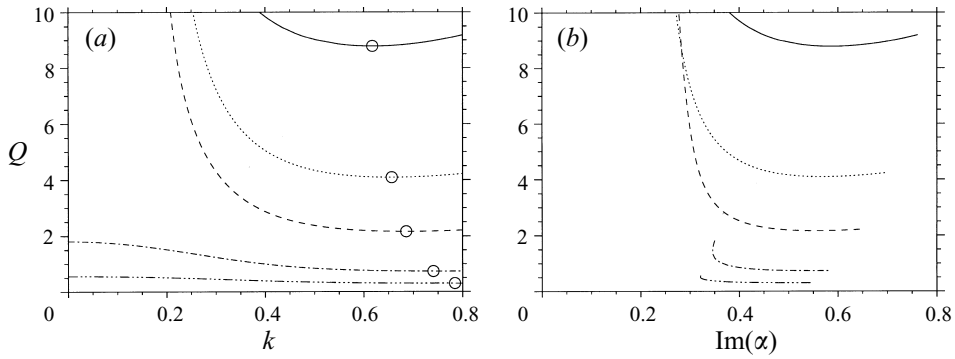

FIGURE 30. Low-frequency neutral stability curves showing (*a*) Q vs. k and (*b*) Q vs. Im(α) with $E = 0$ (solid line), $E = 5$ (dotted line), $E = 10$ (dashed line), $E = 15$ (dash-dot line) and $E = 25$ (dash-dot-dot-dot line), $\gamma = 1.2$ and $f = 1.2$. The circles indicate Q minima in the curves, below which stability prevails.

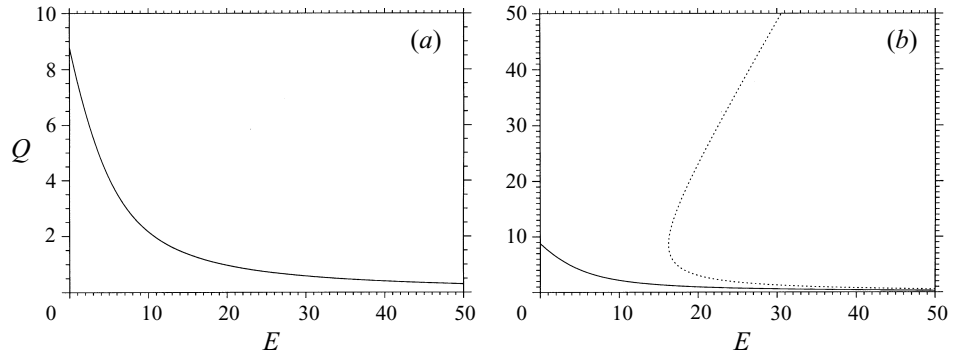

FIGURE 31. (*a*) The Q, E low-frequency two-dimensional neutral stability boundary for $\gamma = 1.2$ and $f = 1.2$. The region to the right of the curve is two-dimensional unstable. (*b*) The Q, E low-frequency two-dimensional (solid line) and one-dimensional (dotted line) neutral stability boundaries. The region to left of the solid line is two-dimensional stable, to the right of the solid line two-dimensional unstable, and to the right of the dotted line one-dimensional unstable.

each mode. For increasing activation energy, smaller amounts of exothermicity are required to generate instability. For the less sensitive reactions, i.e. at lower values of E, a moderately large amount of exothermicity is required to generate two-dimensional instability. Figure 31 shows the low-frequency neutral stability boundary for two-dimensional instability in the (Q, E)-plane for $\gamma = 1.2$ and $f = 1.2$. The region to the right of the curve has a finite region of two-dimensional instability. Figure 31(*b*) also shows the low-frequency neutral stability boundary for one-dimensional instability. The region to the right of the dotted line is one-dimensionally unstable.

Figure 32 shows the same two-dimensional neutral stability boundary plotted in the (β, θ)-plane. We emphasize that β and θ should be better indicators of the stability behaviour since for a given overdrive f and ratio of specific heats γ, it is the relative size of these parameters which reflects the actual sensitivity of the reaction rate to thermodynamic fluctuations, as well as governing the size of the thermodynamic variation in the steady state between the shock and equilibrium point. Figure 32(*a*) shows that for small β, a large value of θ is required to generate a two-dimensional instability. As β increases, smaller values of θ are required to generate instability.

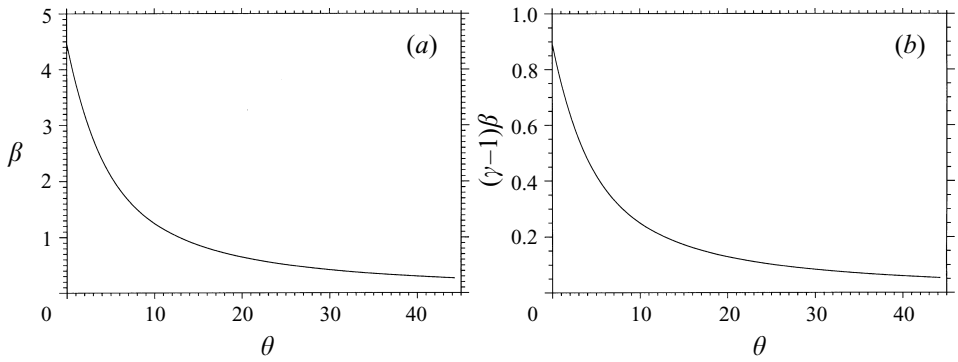

FIGURE 32. (*a*) The β, θ low-frequency two-dimensional neutral stability boundary for $\gamma = 1.2$ and $f = 1.2$. The region to the right of the curve is two-dimensional unstable. (*b*) The $[(\gamma - 1)\beta]$, θ low-frequency two-dimensional neutral stability boundary for $\gamma = 1.2$ and $f = 1.2$.

Figure 32(*b*) shows the neutral stability boundary plotted in the $((\gamma - 1)\beta, \theta)$-plane for the moderately low value of the Newtonian parameter $(\gamma - 1) = 0.2$ used here. The significant practical feature of these results is that regardless of the activation energy, reactive mixtures can always be chosen with sufficiently high levels of inert diluent, thus effectively lowering the value of β, so that the detonation parameters characterizing the mixture will lie close to a neutral stability boundary. In contrast, as shown in §6.1 and §6.2, mixtures in which the detonation is hypersonically driven or have a low degree of reaction sensitivity, characterized by a low value of θ, cannot in themselves ensure that the parameters characterizing the mixture will lie close to a neutral stability boundary.

7. Summary

The hydrodynamic stability to transverse linear disturbances of a steady, one-dimensional detonation in an ideal gas undergoing an irreversible, unimolecular reaction with an Arrhenius rate constant has been investigated for varying bifurcation parameters and in relation to the observed change in the underlying steady wave structure. The results significantly extend those obtained earlier by Erpenbeck. The pre-shock, thermal-energy-scaled activation energy E and heat release Q are found to be poor indicators of the underlying steady wave structure, and those of the detonation-velocity-dependent, post-shock, thermal-energy-scaled activation energy θ and heat release β are found to be more appropriate parameters to explain the linear stability behaviour.

When the steady wave approaches a square-wave-like structure, the linear stability spectrum is found typically to comprise a few modes of two-dimensional higher frequency instability, in addition to a single lower frequency mode of instability. Each mode is found to possess a finite wavenumber band of instability, with stability prevailing above a critical, typically large wavelength W. Given the range of non-local unstable wavenumbers which can be excited, it is possible that the complex linear stability response in such cases can underlie multi-scale, irregular detonation cell formation. For increasing detonation overdrive, or decreasing activation energy, the spatial scale characterizing the underlying steady detonation wave and its main heat release layer increases, and the higher frequency modes sequentially decay. The mode which determines the global maximum growth rate also switches from a range of

higher frequency modes to the lower frequency mode, while the maximum growth rate decreases in amplitude. The range of wavenumbers which are unstable also decreases. Decreases in the activation energy or increases in detonation overdrive for moderate values of the heat release cannot guarantee stability of the steady detonation wave to transverse linear disturbances, and it is always the lowest frequency mode which is found to remain unstable. Stability of the steady detonation wave to two-dimensional linear disturbances appears only to be guaranteed in the limit of sufficiently small heat release, where the steady structure is an inert-Euler step shock for zero heat release. The perturbation eigenfunction structures associated with the mode of lowest frequency instability illustrate multi-scale differences in the spatial behaviour at the low-wavenumber neutral stability point, at the wavenumber corresponding to the point of the maximum growth rate and at the high-wavenumber neutral stability point. When the linear stability response consists of a single, simple mode of low-frequency instability, standard linear stability arguments indicate the subsequent possible emergence of regular detonation cells.

In summary, the results obtained here capture the general trends in the complex two-dimensional linear stability response of a steady, planar detonation wave for the three important bifurcation parameters: the detonation overdrive, the chemical heat release and the activation energy of the Arrhenius chemical reaction. This knowledge will be of significant use in attempts to develop both analytical and numerical models of the onset of the regular and irregular nonlinear cellular detonation patterns that are observed experimentally.

M.S. was supported by the US Air Force Office of Scientific Research (F49620-96-1-0260). D.S.S. was supported by the US Air Force Wright Laboratories (F08630-94-10004) and the US Air Force Office of Scientific Research (F49620-93-1-0532). M.S. is grateful for discussions with Professor P. A. Blythe on the steady detonation wave structure in the limit of low heat release.

Appendix. The linear stability of a step shock in a non-reactive Euler flow

The linear stability of a step-shock wave in a non-reactive Euler flow for an arbitrary equation of state has been investigated by many authors and is governed by the dispersion relation (Buckmaster & Ludford 1986)

$$\alpha^2 A + k^2 M_s^{*2}(\mu - 1) - \alpha M_s^* B \left[\alpha^2 + k^2\left(1 - M_s^{*2}\right)\right]^{1/2} = 0, \tag{A1}$$

where, as before, M_s^* is the post-shock steady flow velocity, μ is the density ratio across the shock, α and k are the disturbance eigenvalue and wavenumber in a normal-mode formulation, A and B are constants given by

$$\left.\begin{aligned} A &= (1-\mu^{-1})\left[\left(1+M_s^{*2}\right) - (\mu-1)\Gamma M_s^{*2}\right] / \left(1-M_s^{*2}\right), \\ B &= (1-\mu^{-1})\left[(\mu-1)\Gamma M_s^{*2} - 2\right] / \left(1-M_s^{*2}\right), \end{aligned}\right\} \tag{A2}$$

and Γ is the Gruneisen coefficient. The equation is a quadratic in α^2/k^2 and thus can be explicitly solved for α/k as a function of μ, M_s^* and Γ. Stability inequalities associated with the dispersion relation have been obtained by Erpenbeck (1962*b*), Majda & Rosales (1983) and Majda (1987) and the following summary is given in Buckmaster & Ludford (1986). First, Erpenbeck (1962*b*) showed that for

$$(\mu - 1)M_s^* > (1 + M_s^*)\Gamma^{-1} \tag{A3}$$

$\alpha > 0$ and real. Secondly, Majda & Rosales (1983) showed that for

$$(\Gamma + 1)^{-1} \leqslant (\mu - 1)M_s^2 < (1 + M_s)\Gamma^{-1} \tag{A4}$$

α is purely imaginary, and finally Majda (1987) showed that for

$$(\mu - 1)M_s^2 < (\Gamma + 1)^{-1} \tag{A5}$$

the step shock is stable with $\mathrm{Re}(\alpha) < 0$.

For an ideal gas, the Gruneisen coefficient is given by

$$\Gamma = \gamma - 1 \tag{A6}$$

and it can be shown that for a finite, steady shock propagation Mach number D^*, the relation (A5) is always satisfied.

REFERENCES

Barthel, H. O. 1974 Predicted spacings in hydrogen-oxygen-argon detonations. *Phys. Fluids* **17**, 1547–1553.

Barthel, H. O. & Strehlow, R. A. 1966 Wave propagation in one-dimensional reactive flows. *Phys. Fluids* **9**, 1896–1907.

Bourlioux, A. & Majda, A. J. 1992 Theoretical and numerical structure for unstable two-dimensional detonations. *Combust. Flame* **90**, 211–229.

Bourlioux, A., Majda, A. J. & Roytburd, V. 1991 Theoretical and numerical structure for unstable one-dimensional detonations. *SIAM J. Appl. Maths* **51**, 303–343.

Buckmaster, J. D. 1989 A theory for triple point spacing in overdriven detonation waves. *Combust. Flame* **77**, 219–228.

Buckmaster, J. D. & Ludford, G. S. S. 1986 The effect of structure on the stability of detonations I. Role of the induction zone. In *Twenty-first Symp. (Intl) on Combustion,* pp. 1669–1676. The Combustion Institute.

Clavin, P. & He, L. 1996 Stability and nonlinear dynamics of one-dimensional overdriven detonations in gases. *J. Fluid. Mech.* **306**, 353–378.

Erpenbeck, J. J. 1962*a* Stability of steady-state equilibrium detonations. *Phys. Fluids* **5**, 604–614.

Erpenbeck, J. J. 1962*b* Stability of step shocks. *Phys. Fluids* **5**, 1181–1187.

Erpenbeck, J. J. 1964 Stability of idealized one-reaction detonations. *Phys. Fluids* **7**, 684–696.

Erpenbeck, J. J. 1965 Stability of idealized one-reaction detonations: zero activation energy. *Phys. Fluids* **8**, 1192–1193.

Erpenbeck, J. J. 1966 Detonation stability for disturbances of small transverse wavelength. *Phys. Fluids* **9**, 1293–1306.

Erpenbeck, J. J. 1970 Nonlinear theory of two-dimensional detonations. *Phys. Fluids* **13**, 2007–2026.

Fickett, W. & Davis, W. C. 1979 *Detonation.* University of California Press.

Fickett, W. & Wood, W. W. 1966 Flow calculations for pulsating one-dimensional detonations. *Phys. Fluids* **9**, 903–916.

Kaneshige, M., Shepherd, J. E. & Teodorczyk, A. 1997 Detonation database. Graduate Aeronautical Laboratories, California Institute of Technology.

Lee, H. I. & Stewart, D. S. 1990*a* Calculation of linear instability: one-dimensional instability of plane detonation. *J. Fluid Mech.* **216**, 103–132.

Lee, H. I. & Stewart, D. S. 1990*b* Calculation of linear instability: two-dimensional instability of plane detonation. Presented at *the 10th Intl Workshop on Mathematics in Combustion, University of Poitiers, France.*

Lee, J. H. S. 1984 Dynamic parameters of gaseous detonations. *Ann. Rev. Fluid Mech.* **16**, 311–336.

Majda, A. J. 1987 Criteria for regular spacing of reacting Mach stems. *Proc. Natl Acad. Sci. USA* **84**, 6011–6014.

Majda, A. J. & Rosales, R. 1983 A theory for spontaneous Mach Stem formation in reacting shock fronts. I: the basic perturbation analysis. *SIAM J. Appl. Maths* **43** 1310–1334.

Majda, A. J. & Roytburd, V. 1992 Low-frequency multidimensional instabilities for reacting shock waves. *Stud. Appl. Maths* **87**, 135–174.

Quirk, J. J. 1994 Godunov-type schemes applied to detonation flows. In *Combustion in High-speed Flows* (ed. J. Buckmaster, T. L. Jackson & A. Kumar), pp. 575–596. Kluwer.

Quirk, J. J. & Short, M. 1998 Cellular detonation stability. Part 2. The dynamics of cell formation. In preparation.

Short, M. 1996 An asymptotic derivation of the linear stability of the square wave detonation using the Newtonian limit. *Proc. R. Soc. Lond.* A **452**, 2203–2224.

Short, M. 1997*a* Multi-dimensional linear stability of a detonation wave at high-activation energy. *SIAM J. Appl. Maths* **57**, 307–326.

Short, M. 1997*b* A parabolic linear evolution equation for cellular detonation instability. *Combust. Theory Modell.* **1**, 313–346.

Short, M. & Quirk, J. J. 1997 On the nonlinear stability and detonability limit of a detonation wave for a model 3-step chain-branching reaction. *J. Fluid Mech.* **339**, 89–119.

Short, M. & Stewart, D. S. 1997 Low-frequency two-dimensional linear instability of plane detonation. *J. Fluid Mech.* **340**, 249–295.

Stewart, D. S., Aslam, T. D. & Yao, J. 1996 On the evolution of cellular detonation. In *Twenty-sixth Symp. (Intl) on Combustion.* pp. 2981–2989. The Combustion Institute.

Strehlow, R. A. 1969 The nature of transverse wave in detonations. *Astron. Acta* **14**, 539–548.

Strehlow, R. A. 1970 Multi-dimensional detonation wave structure. *Astron. Acta* **15**, 345–357.

Strehlow, R. A. & Crooker, A. J. 1974 The structure of marginal detonation waves. *Acta Astron.* **1**, 303–315.

Strehlow, R. A. & Fernandes, F. D. 1966 Transverse waves in detonations. *Combust. Flame* **9**, 109–119.

Strehlow, R. A., Maurer, R. E. & Rajan, S. 1969 Transverse waves in detonations: I. Spacing in the hydrogen-oxygen system. *AIAA J.* **7**, 323–328.

Yao, J. & Stewart, D. S. 1996 On the dynamics of multi-dimensional detonation waves. *J. Fluid Mech.* **309**, 225–275.